Zebrafish xenograft model: Identification of novel mechanisms driving prostate cancer metastasis

Chen, L.

Chapter 5

A NF-κB-Activin A signaling axis enhances prostate cancer metastasis

Lanpeng Chen[1], Marta De Menna[2], Arwin Groenewoud[1], George N. Thalmann[3], Marianna Kruithof-de Julio[2*] and B. Ewa Snaar-Jagalska[1*]

[1]Institue of Biology, University of Leiden, Leiden, NL

[2]Department of BioMedical Research, Urology Research Laboratory, University of Bern, Bern, CH

[3]Department of Urology, Inselspital, Bern, CH

* Corresponding Authors

PD. Dr. Marianna Kruithof-de Julio, marianna.kruithofdejulio@dbmr.unibe.ch

Prof. B. Ewa Snaar-Jagalska, b.e.snaar-jagalska@biology.leidenuniv.nl

Oncogene, 2020, 39(8), 1634.

Abstract

Metastasis is a main cause of death in prostate cancer (PCa). To dissect the molecular cues from cancer cell-microenvironment interaction that drive metastatic cascade, bone metastatic PCa cells were intravenously implanted into zebrafish embryos and mice tibia forming metastatic lesions. Transcriptomic analysis showed an elevated expression of stemness genes, pro-inflammatory cytokines and TGF-β family member Activin A in the cancer cells at metastatic onset in both animal models. Consistently, analysis of clinical datasets revealed that the expression of Activin A is specifically elevated in metastases and correlates with poor prognosis in stratified high risk PCa patients. It is further unveiled that the microenvironment induced Activin A expression by NF-κB activation. The elevated level of Activin A enhanced the invasive ALDH^{hi} CSC-like phenotypes and PCa proliferation by activation of Smad and ERK1/2 signaling driving metastasis. Suppression of Activin A or Activin receptor significantly reduced the CSC-like subpopulation, invasion, metastatic growth and bone lesion formation in zebrafish and mice xenografts, suggesting a functional role of NF-κB dependent Activin A in PCa metastasis. Overall, our study demonstrates that human PCa cells can display a comparable response to the microenvironment in zebrafish and mice xenografts. Combining both animal models, we uncovered the microenvironment-dependent activin signaling as an essential driver in PCa metastasis with therapeutic potential.

Introduction

Prostate cancer (PCa) is the second most prevalent cancer in males around the world[1]. However, in 20-30% of patients with apparently organ-confined prostate carcinoma, beneficial responses are followed by tumor recurrence at distant sites leading to incurable, devastating metastatic disease. Prostate cancer metastases may originate from small cellular subpopulation, cancer stem-like cells (CSCs). These cells display high expression of certain stem cell markers including CD44, α2β1 and Aldehyde dehydrogenases (ALDHs)[2,3]. It is well documented that the ALDH^{hi} subpopulation of PCa isolated by viable cell sorting display CSCs characteristics[4]. Although the features of prostate CSCs have been explored in the past decade, it is still unknown how these cells respond to the microenvironment and initiate metastatic outgrowth after extravasation.

Activin and Nodal are extracellular proteins belonging to TGF-β superfamily[5]. Both ligands bind to activin-like type II receptor ACVR2a and/or ACVR2b and lead to the signal transduction through the type I receptor ALK4, which subsequently induces Smad2/3 phosphorylation and Smad4 activation[6]. Additionally, Activin/Nodal downstream signaling displays a cross-talk with MAP kinase pathway[7,8]. Functionally, Activin/Nodal plays a critical role in maintaining pluripotency of stem cells, mesoderm formation and left-right axis specification in human[9,10,11,12]. Moreover, contribution of Activin/Nodal signaling in cancer progression has been reported[13]. Nodal together with its co-receptor Cripto drive self-renewal and tumorigenicity of pancreatic, prostate and liver cancer stem cells[14,15, 16,17,18]. In breast, lung

and gastric cancer, Activin A, a protein dimer formed by INHBA, has a pro-metastatic function[19,20,21,22]. However, the role of Activin in prostate cancer is still controversial. Activin was originally identified as a tumor suppressor to block cell cycle progression through the activation of Smad signaling pathway [23,24]. However, this anti-proliferative effect is missing in the late stage of the disease[25,25] as high levels of circulating activin in the patients with bone metastasis is no longer able to restrain disease progression[5]. A previous study indicated elevated levels of circulating Activin in the patients with bone metastasis, suggesting that Activin might play an oncogenic role in the late stages of the disease, presumably by controlling aggressive behavior of CSCs [26].

In order to identify molecular cues involved in cancer cell-microenvironment interaction driving metastatic process, we injected human PCa cells into zebrafish embryos and in the mice tibia. Transcriptomic analysis of PCa cells in culture compared to cells which formed experimental metastases demonstrated increased levels of stemness, pro-inflammatory cytokines and Activin signaling genes in both *in vivo* models. In line with patient data, the expression of Activin A was elevated in zebrafish and mice xenografts, suggesting that independent of host species, the underlying mechanism that governs Activin A expression remains conserved and is driven by heterogeneity of the microenvironment. Our study revealed that NF-κB dependent Activin A expression controls the CSC-like properties through activation of Smad signaling and drives cell proliferation by elevating ERK1/2 phosphorylation. Genetic and pharmacological inhibition of Activin A or Activin receptors in PCa cells significantly suppressed the size of $ALDH^{hi}$ CSC-like subpopulation, invasion, metastatic growth and bone lesion formation in both *in vivo* models. Our study highlights the role of NF-κB - dependent Activin A signaling in prostate cancer metastasis and suggest that Activin signaling could be a potent target for the treatment of late stage PCa.

Materials and methods

Analysis of publicly available dataset of PCa patients

Gene expression-based survival/recurrence analysis was performed with SurvExpress, an online biomarker validation tool (http://bioinformatica.mty.itesm.mx/SurvExpress)[27]. Gene expression between primary site and metastasis was extracted with Oncomine (Compendia Bioscience).

Cell lines and *in vitro* treatment

Human embryonic kidney cells HEK-293T (kindly provided by Dr. Sylvia Le Dévédec, LACDR, Leiden), human prostate cancer cells PC-3 and PC-3M-Pro4 (kindly provided by Dr. Gabriel van der Pluijm, Department of Urology, LUMC) were cultured as previously described[18]. In brief, HEK-293T cells were maintained in Dulbecco's modified Eagle's medium (DMEM) supplemented with 10% FCS. PC-3 were cultured in Dulbecco's Modified Eagle Medium: Nutrient Mixture F-12 (DMEM/F-12) Media (Gibco™) supplemented with 10% FCS and L-

glutamine. PC-3M-Pro4 were maintained in DMEM supplemented with 10% FetalClone II (Hyclone™). C4-2B were maintained in low-glucose DMEM (Gibco™) supplemented with 20% Ham's F-12K (Sigma), 10% FCS, 1xITS Liquid Media Supplement (Thermo Fisher Scientific), 13,6pg/ml T3, 0,25ug/ml Biotin and 25ug/ml Adenine. All cells used in the research were authenticated by STR (Microsynth's cell line authentication service, Bern, Switzerland) and past mycoplasma test using Mycoplasma Test Kit (ATCC). For 3D cultures, cells were grown in ultra-low attachment multiwell plates (Corning Costar) in the medium as mentioned above. For compounds stimulation or inhibition, cells were seeded in 6-well plates in the complete medium with a concentration of 80,000 cells/well. One day after seeding, the full medium was refreshed with serum-starvation medium containing 3% serum. Human recombinant TNFα, human recombinant activin A, human recombinant IL-8 and human recombinant TGF-β were all purchased from Thermo Fisher Scientific. ALK inhibitor SB-431542, ALK inhibitor SB-505124 and ERK1/2 inhibitor SCH772984 were purchased from Cayman Chemical. Each compound was used either alone or in combination. The final concentrations of use are reported in the figure legends.

Zebrafish maintenance, tumor cell implantation and metastasis analysis

Tg(Fli:GFP[28] and Mpeg:GFP[29]) Zebrafish (ZF) were handled and maintained according to standard protocols (www.ZFIN.org). Experiments were assessed by Animal Experiments Committee (Dier Experimenten Commissie – DEC) and assessed by Central Committee on Animal Testing (CCD) under licence UDEC 14227 and AVD1060020172410.

For cancer cell transplantation, two days post-fertilization (dpf), dechorionated zebrafish embryos were anaesthetized with 0.003% tricaine (Sigma) and plated on a 10cm Petri dish covered with 1.5% of solidified agarose. Cancer cells were suspended in PBS containing 2% polyvinylpyrrolidone (PVP; Sigma-Aldrich) with a concentration of 50,000 cells/ul and loaded into borosilicate glass capillary needles (1 mm O.D. × 0.78 mm I.D.; Harvard Apparatus). 200-400 human cancer cells were injected into the duct of cuvier (DoC) of the zebrafish embryos using a Pneumatic Picopump and a manipulator (WPI). After transplantation, the embryos were incubated in a 34 ˚C incubator. For each time of imaging analysis, 30 fish per group was randomly selected from large groups(>120 engrafted embryos) to avoid variation. Images were acquired at 1-, 2-, 4- and 6-days post injection (dpi) with a Leica M165 FC stereo fluorescent microscope[32]. Cancer cell burden at the metastatic site was blindingly quantified by calculating the total mCherry fluorescence at CHT area with the ZF4 pixel counting program (Leiden)[30]. Each experiment was performed at least 2 times with a group size of 30 as previously described [18].

For high resolution imaging, zebrafish embryos were placed on glass-bottom petri dishes and covered with 1% low melting agarose containing 0.003% tricaine (Sigma). Imaging was

performed using the Leica SPE confocal microscope or Nikon Eclipse Ti confocal laser-scanning microscope. The images were processed with imageJ software.

RNA extraction and qPCR

80 fish/group was randomly selected from the large group (>120 fish per group). Metastases tissue were isolated by cutting the whole metastatic area at 6dpi with a micro dissection scissor (WPI). The samples were immediately washed with cold PBS and stored in TRIzol (Sigma) at -80 ˚C. The whole process was finished within 30 min. Total RNA from paraffin sections of bone metastasis was isolated using the FFPE RNAeasy isolation kit from QIAGEN according to manufacturer's instructions. Whole RNA was isolated using the RNeasy mini kit (qiagen) following the manufacturer's protocol. For cDNA synthesis and qPCR, iScript™ cDNA Synthesis Kit (Bio-Rad) and iQ™ SYBR® Green Supermix (Bio-Rad) were used following the manufacture's protocol. For each gene analyzed human specific primers were designed in order to measure the gene expression variation in human cancer cells. The species-specificity was tested before the experiments. GAPDH and/or β-actin were included as housekeeping for normalization. Three independent experiments were performed.

RNA-seq sequencing and data analysis

RNA samples (80 fish per sample with 3 samples per condition from independent experiment) were collected as mentioned above. RNA quality assessment and sequencing was performed at ZF-screen (Leiden, The Netherlands). Integrity of the RNA was confirmed using an Agilent Bioanalyzer 2100 and RNA 6000 Nano or Pico kit (Agilent, Amstelveen, Netherlands). The SMART-Seq v4 Ultra low input RNA kit (Takara Bio Europe) was used to prepare cDNA and then Illumina RNAseq libraries were prepared using the Illumina TruSeq RNA Sample Prep Kit v2 according to the manufacturer's instructions (Illumina, San Diego CA, USA). All RNAseq libraries (150–750 bp inserts) were sequenced on an Illumina HiSeq2500 sequencer as 1 × 50 nucleotides single-end reads according to the manufacturer's protocol. Image analysis and basecalling were done using the Illumina pipeline. Total yield varied from 10 to 26 Mreads per sample. Illumina reads were aligned against the human (GRCh38.p3) and zebrafish (GRCz10.80) reference genome sequences using TopHat (version 2.0.5)[31]. Secondary alignments of reads were excluded by filtering the files using SAMtools (version 0.1.18)[32]. Aligned fragments per predicted gene were counted from SAM alignment files using the Python package HTSeq (version 0.5.3p9)[33]. To make comparisons across samples possible, these fragment counts were corrected for the total amount of sequencing performed for each sample. As a correction scaling factor, library size estimates determined using the R/Bioconductor (release 2.11) package DESeq were employed[34]. Read counts were normalized by dividing the raw counts obtained from HTSeq by its scale factor. Detailed read coverage for individual genes was extracted from the TopHat alignments using SAMtools. Sequencing data has been submitted to Gene Expression Omnibus (GEO) with an accession code GSE137629. DAVID Bioinformatics Resources 6.8 (NIAID/NIH) and Gene Set Enrichment Analysis (BROAD institute) were eventually used for gene profile analysis.

Immunofluorescence

Whole mount immunofluorescence on zebrafish embryos was conducted as previously described[30]. After fixation with 4% PFA, embryos were dehydrated and rehydrated with methanol in series concentration (25%, 50%, 75% and 100%). After permeabilization with 10ug/ml Protease K, embryos were blocked within blocking buffer containing 0.7%Triton X-100 and 5% sheep serum in 0.5% PBST. After incubation with primary (1/200) and fluorescence-conjugated secondary (1/200) antibodies images were acquired using Leica SPE or Nikon Eclipse Ti confocal laser-scanning microscope. Antibodies included rabbit anti-human Ki67 (Abcam, ab15580), anti-human phospho-Histone3 (Santa Cruz, SC-8656-R), anti-human P65 (Cell Signaling Technology, CST8242), anti-human phospho-P65 (Ser536) (Cell Signaling Technology, CST3033), anti-human INHBA (Abcam, ab56057) and anti-phosphor-Smad2 (Ser465/467) (kindly provided by Prof. Peter ten Dijke, Department of Molecular Cell Biology, LUMC).

Western blot

Cells were lysed with Lysis buffer complemented with protease inhibitor (Cell Signaling Technology). Samples were separated by SDS-PAGE (Bio-Rad) and transferred to polyvinylidene difluoride membranes (Millipore), incubated with primary antibodies (1:1000 times dilution) followed by horseradish peroxidase-labeled secondary antibodies (1:1000 times dilution) (Cell Signaling Technology), and developed with enhanced chemiluminescence substrate mixture (Cell Signaling Technology). Blots were scanned on a Typhoon 9400 (GE Healthcare). Rabbit anti-human GAPDH (Santa Cruz Biotechnology, SC-32233), Rabbit anti-human P65 (Cell Signaling Technology, CST8242), anti-human phosphor-P65 (Ser536) (Cell Signaling Technology, CST3033), anti-human INHBA (Abcam, ab56057), anti-human ERK1/2 (Cell Signaling Technology, CST137F5), anti-human phosphor-ERK1/2 (Thr202/Tyr204) (Cell Signaling Technology, CST4370) and anti-human phosphor-Smad2 (Ser465/467) (Kindly provided by Prof. Peter ten Dijke, Department of Molecular Cell Biology, LUMC) were used.

3D collagen invasion assay

Collagen gel was prepared from collagen type I stock (BD, Bioscience) with a final concentration of 1mg/ml in 44 mM NaHCO3, 0.1M Hepes (BD, Bioscience) and 1X pen/strep (Gibco™). mCherry labeled cancer cells were suspended in PBS containing 2% polyvinylpyrrolidone (PVP; Sigma-Aldrich) to 50,000 cells/ul and loaded into borosilicate glass capillary needles (1 mm O.D. × 0.78 mm I.D.; Harvard Apparatus). 10,00 cells/drop were injected into the prepared solidified 3D collagen gel in 6 well plates with use of an air-driven microinjector (20 psi, PV820 Pneumatic PicoPump; World precision Inc). Tumor spheres were imaged at day 0 and day 3 with a Leica M165 FC stereo fluorescent microscope. The number of invading cells was calculated by measuring the number of fluorescent cells surrounding

central tumor mass with ImageJ image analysis software; 10-15 tumor spheres were measured in each condition.

Cell proliferation assay

Cell proliferation was assessed with Cell Proliferation Reagent WST-1 (Roche) following the manufacturer's protocol. In brief, 6000 cells in 100uL full medium were seeded in each well of a 96 wells plate. After 24h the medium was replaced with low serum medium (3% serum) containing either Vehicle (Veh) control, cytokines or inhibitors. Cells were allowed to grow for 24, 48 and/or 72 hours. For measurement, 10uL/well WST-1 reagent was added followed by 2 hours incubation at 37 ˚C. Each condition was repeated 6 times in two independent experiments. Measurement was performed with microplate reader M1000 PRO (TECAN).

Clonogenicity Assay

Single cells were seeded in a 6 wells plate (200 cells/well) covered with 1.5ml completed medium. After 10 days the cells were stained with crystal violet following fixation with 4% Paraformaldehyde (PFA). After imaging, number and/or size of the colonies per well were determined through ImageJ data analysis. Each experiment was independently repeated 3 times.

ALDEFLUOR assay and FACS sorting

Aldehyde dehydrogenase (ALDH) activity of the cells was measured with use of ALDEFLUOR Assay kit (StemCell technology) following the manufacturer's protocol. Flow cytometric (FACS) measurement and sorting were performed as described before[3]. Briefly, 1-10 million PC-3M-Pro4-mCherry cells were treated with the ALDEFLUOR reagent. As a negative control 500.000 PC-3M-Pro4-mCherry cells were first treated with ALDEFLUOR reagent and then immediately with DEAB, an ALDH inhibitor. These cells were used to set the gate for the negative population. FACSCanto II (BD Biosciences) was used for the measurement and data was further analyzed with FCS Express Software (De Novo Software). Each condition was independently repeated 3 times.

Gene interference with shRNAs

Short hairpin RNA (shRNA) constructs (clone# TRCN0000376721 (INHBAkd1), TRCN0000376723 (INHBAkd2), TRCN0000010321 (SMAD4 kd1), TRCN0000010322 (SMAD4 kd2), and SHC002 (Scramble (SCR) control) were obtained from Sigma's MISSION library (Kindly provided by Department of Molecular Cell Biology, LUMC). Lentivirus were produced by transforming short hairpin constructs, packaging plasmids psPAX2 and enveloped plasmids pMD2.G with a ratio of 3:2:1 using lipoD293 (SignaGen Laboratories) as transfection reagent. Lentiviral supernatant was collected 72 hours after transformation. Cells were transduced with the lentivirus in presence of 6ug/ml Polybrene (Sigma-Aldrich). Transduced cells were maintained in the complete medium with 1ug/ml Puromycin for selection (Sigma-Aldrich).

Mice experiment

Male 5-6 weeks old CB17 SCID mice, were purchased from Charles River (L'Arbresle, France) and housed in ventilated cages under sterile condition. Sterile food and water was provided *ad libitum*. Animal experiments were performed in accordance with Swiss Guidelines for the Care and Use of Laboratory Animals under the license BE55/16 approved by the local committee for animal health ethics and research of the Canton Bern, Switzerland. Intra-osseous (IO) experiments were performed as previously described[35]. 50.000 PC-3M-Pro4-LUC2-mCherry bearing either a stable shRNA knockdown for INHBA or a scramble shRNA as a control were injecting in the left tibia of the mice (5 mice per group). BLI imaging (NightOwl, Berthold, Bad Wildbad, Germany) and X-ray assessment (Faxitron Bioptics, Tucson, Arizona, US) at day 7, 14 and 28 after implantation were conducted in blinding respectively for all of the engrafted mice to track cell growth and bone lesions progression.

Statistics

Statistics analysis was performed with Graphpad Prism 7.0 (San Diego, CA, USA). Outliers were tested and excluded using ROUT method (Q=0.1%). F- test was performed to compare variation of each groups. t-Test was used to compare two groups and ANOVA for multiple groups. Data is presented as mean ±SEM or mean ±SD. p-values ≤0.05 are considered to be statistically significant (*p≤0.05, **p<0.01, ***p<0.001, ****P<0.0001)

Results

Intravenous transplantation of prostate cancer cells into zebrafish embryos induces metastatic tumor growth associated with enhanced expression of gene signatures for cancer stemness, NF-κB and Activin signaling

To visually trace the metastatic onset of PCa cells, we established a zebrafish (ZF) xenograft model by intravenously (IV) injecting approximately 500 mCherry-labeled prostate cancer cells through Duct of Cuvier (DoC) into 2 days post fertilization (dpf) zebrafish Tg (fli1: EGFP) embryos with green fluorescent vessels[28] (Fig. 1a). DoC is an open blood circulation channel connecting the heart and the trunk vasculature. This IV transplantation allowed cancer cells passively spread through whole body, extravasate from the caudal vein, invade, proliferate and eventually form extravascular metastasis specifically at the caudal hematopoietic tissue (CHT) area at four to six days after transplantation (Fig. 1b)[36,37,38,39]. We assessed by fluorescence the relative metastatic potential of multiple prostate cancer cell lines including DU145, LNCaP, C4-2B, PC-3 and PC-3M-Pro4. Only PC-3 and PC-3M-Pro4 displayed moderated and advanced metastatic growth respectively, at the CHT hallmarked by collective invasion into the neighboring tissue at 6 days post transplantation (dpi) (Fig. 1b). DU145, LNCaP and C4-2B, however, failed to form metastasis (Supplementary Table 1).

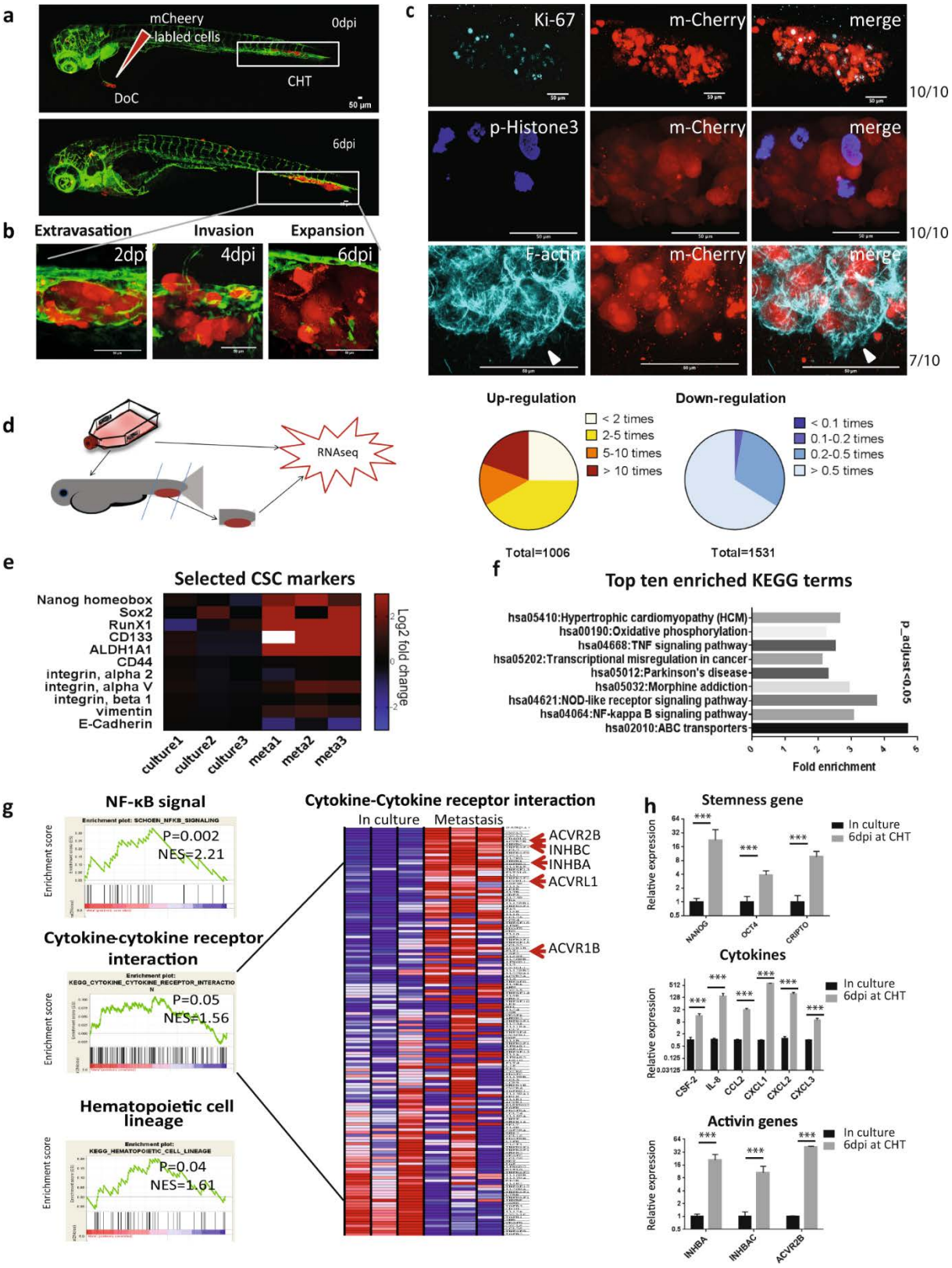

Fig. 1 Intravenous transplantation of prostate cancer cells results in metastatic growth associated with upregulation of stemness genes, NF-κB cytokines and Activin (a) PC-3M-Pro4-mCherry were injected into DoC (Duct of Cuvier) at 2dpf (top image). Micro-metastasis developed at 6dpi (8dpf) at CHT (bottom image) (red, cancer cells; green, zebrafish vessel). (b) Whole process of metastatic onset of PC-3M-Por4 was monitored by high resolution imaging. The cancer cells extravasated from the caudal vein (left) and invaded into the neighboring tissue (middle). At 6dpi clear extravascular micro-metastases were developed (right). (c) Whole

mount immunofluorescence against Ki-67(cyan), phosphorylated-Histone3 (blue) and F-actin (cyan) at 6dpi. In total 10 fish was stained for each group. 10 out of 10 were positive for Ki-67 and phosphorylated-Histone3 in the metastasized cancer cells. 7 out of 10 were positive for elongated protrusions at the invasive front. Scar bar=50um. Arrow, Actin protrusions. (d) RNAseq analysis for comparison of PC-3M-Pro4 cultured *in vitro* with PC-3M-Pro4 isolated from ZF CHT at 6dpi. 2536 genes were found differentially expressed: 1006 genes upregulated and 1531 downregulated (p-adjust<0.05). (e) RNAseq showed upregulation of Stemness genes NANOG, SOX2, RUNX1, CD133, ALDH1A1, Integrin αV and EMT marker Vimentin in metastasis (fold change>2, p<0.05) While the epithelial marker E-cadherin was down-regulated (fold change<0.5, p<0.05). (f) Gene onthology analysis was performed using DAVID Bioinformatics Resources 6.8, NIAID/NIH. Top ten KEGG Pathway terms enriched in metastasis are displayed(p<0.05). (g) Gene Set Enrichment Analysis was performed to analyze the modification of signaling pathways. NF-κB signaling, Cytokine-Cytokine receptor interaction and Hematopoietic cell lineage were upregulated in the metastases (left) (p<0.05). Activin subunits INHBA, INHBC and Activin receptors were present in the gene set Cytokine-cytokine receptor interaction (right). (h) Comparison of CSC markers, NF-κB -related cytokines and Activin components in PC-3M-Pro4-lifeact in culture and in metastases using qPCR (n=3, p<0.001).

Cell division and invasion at the metastatic site at CHT area were characterized by whole mount immunofluorescence. Proliferation of cells was determined by nuclear staining with Ki-67 and phosphorylated histone 3 antibodies (Fig. 1c). Phalloidin staining visualized invadopodia-like protrusions at the invasive front of the metastatic lesion (Fig. 1c).

Prostate osteotropic cancer cells have been reported to specifically target the hematopoietic niche which in turn supports their metastatic growth in mice[40,41]. We examined if the osteotropic PCa cells also responded to the molecular cues from CHT, the ZF hematopoietic niche with molecular similarity to human bone marrow[42]. Illumina RNAseq analysis of both, PC-3M-Pro4 cells in culture and micro-dissected metastatic lesion samples from zebrafish xenografts at 6dpi (80 fish per group and 3 biological repeats) depicted approximately 2500 human genes (P-adjust<0.05) differentially expressed (Fig. 1d). Among these genes: CD133, ALDH1A1, NANOG, SOX2, and Integrin αV and EMT markers Vimentin were significantly upregulated (fold change>2 and p<0.05) whereas the epithelial marker E-cadherin was downregulated (fold change < 0.5 and p<0.05) (Fig. 1e), indicating the cancer cells acquired enhanced stemness and EMT features at metastatic onset in CHT.

We next used DAVID Functional Annotation Tool (NIAID/NIH) to identify signaling pathways modified by the microenvironment in cancer cells forming metastatic lesion. The elevated genes were mainly involved in the inflammatory response, ABC transporters, stress coping and NF-κB activation (Fig. 1f). Gene Set Enrichment Analysis (GSEA, Broad Institute, UC SanDiego) identified the highest enrichment score for TNF Signaling Via NF-κB, Cytokine-Cytokine Receptor Interaction and Hematopoietic cell (NES>1.5 and p<0.05) (Fig. 1g). Interestingly, genes related to Activin/Nodal signaling pathway including Activin A, Activin C (INHBC), Activin type II receptor ACVR2B and Type I receptor ALK4 were significantly upregulated in those gene sets (Fig. 1e, Supplementary Table 2).

QPCR validation of the genes selected by RNAseq analysis confirmed that stemness genes NANOG, OCT4, NF-κB-related cytokines GM-CSF, CCL2, IL-8, CXCL2, Activin signaling components Activin A, Activin C and ACVR2B were upregulated by 10-100 fold in the metastatic lesions (p<0.0001) (Fig. 1h). Importantly, this upregulation was specifically induced

by cues from the microenvironment as it was not induced by shifting cells from 2D culture into 3D spheres (Supplementary Fig. S1).

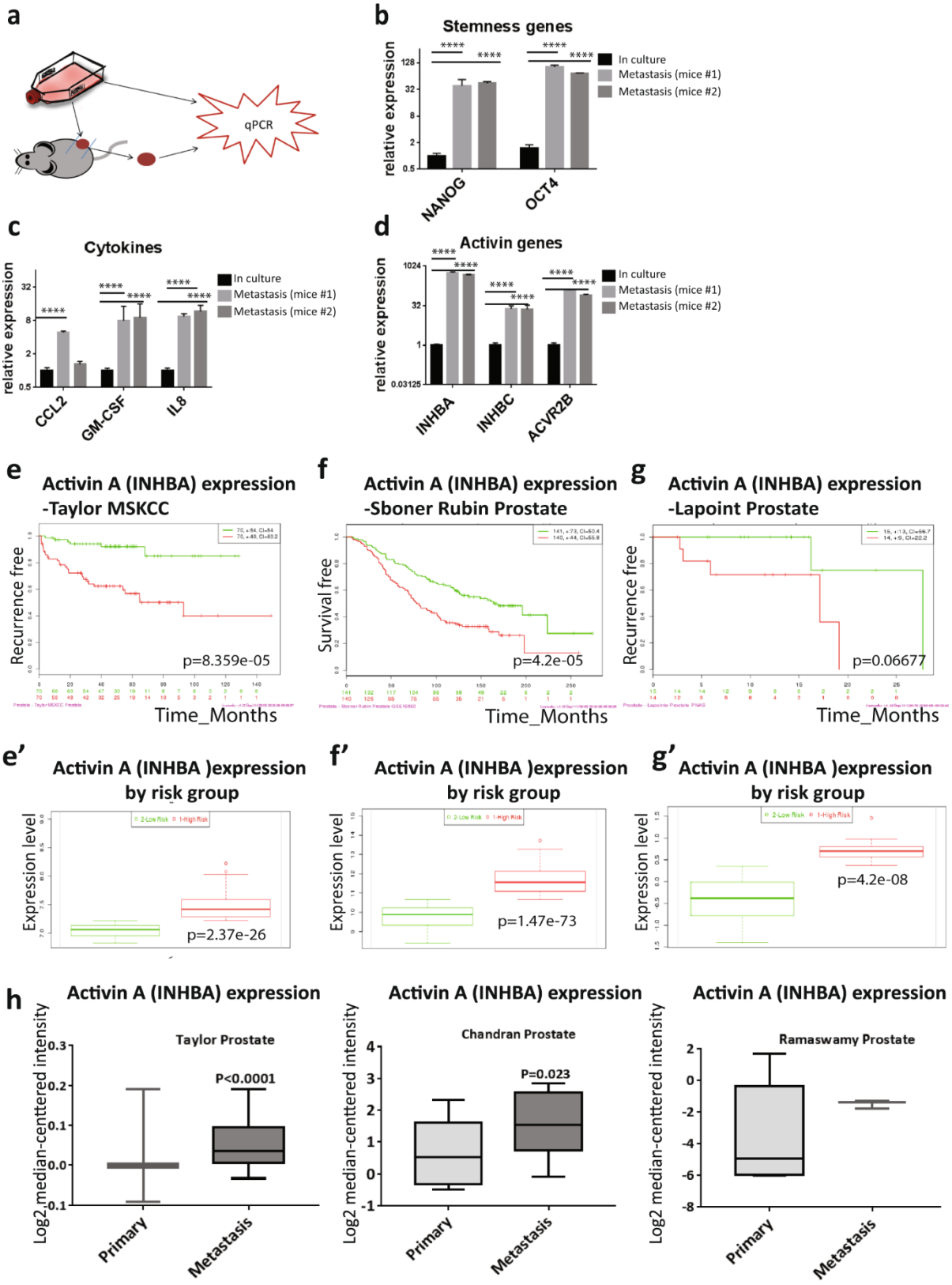

Fig. 2 Activin A is upregulated in metastasis in mice xenografts and correlates with malignant progression in PCa patients. (a) PC-3M-Pro4-Luc2 were intra-osseously engrafted in mice tibia. RNA was isolated from paraffin embedded sections of mice tibias and qPCR was performed to compare gene expression between PC-3M-Pro4-

Luc2 implanted in the bone and PC-3M-Pro4-Luc2 growing in culture. (b) Stemness genes, (c) NF-κB-related cytokines and (d) Activin genes were upregulated in the PC-3M-Pro4-luc2 cells growing- in mice bone (technical repeats=3, $p<0.001$). (e-g) Disease recurrence and patient survival were analyzed with Kaplan-Meier survival curve. Patients with high expression of Activin A (INHBA) (red) have a high probability of recurrence and death in comparison with the low expression one (green) in 3 different clinical datasets including Taylor MSKCC ($p<0.0001$), Sboner Rubin Prostate ($p<0.0001$) and Lapointin Prostate ($p=0.067$). (e'-g') Patients were classified based on risk group in each clinical dataset. The patients with a high risk (red) have significantly high expression of Activin A ($p<0.0001$). (h) Activin A is upregulated in prostate cancer metastases compared with the primary site. Clinical datasets Taylor Prostate, Chandran Prostate and Ramaswamy Prostate are used for analysis (data accessed from www.oncomine.org).

Activin A is upregulated in bone metastases in mice xenografts and correlates with a poor survival and high metastasis risk of PCa patients

To examine if the effect of ZF microenvironment on the gene expression of the PCa cells is comparable with that of mice bone marrow during PCa metastasis, PC-3M-Pro4-LUC2 were injected into mice tibia[43]. 4 weeks post injection, RNA was isolated from the tumor tissues and analyzed with qPCR (Fig. 2a). Consistently with the zebrafish xenografts, significant upregulation of pluripotency genes NANOG, OCT4, NF-κB dependent cytokines CCL2, GM-CSF, IL8, Activin signaling components Activin A (INHBA), Activin C (INHBC) and ACVR2B was detected (Fig. 2b-d). Taken together, our transcriptional analysis proposes that the human cancer cells in ZF microenvironment displayed a similar response as in mice bone marrow. This cell-microenvironment interaction resulted in an augmentation of CSC-like phenotype, NF-κB activation and Activin genes expression.

Activin signaling has been shown to regulate malignant progression of cancer cells in multiple types of carcinomas. However, its role in prostate cancer remains unknown. We next investigate the clinical relevance of this Activin upregulation in PCa progression. Multiple public clinical data sets were analyzed including Taylor MSKCC Prostate GSE21032, Sboner Rubin Prostate GSE16560 and Lapointe Prostate GSE3933. Consistently, all showed high expression of Activin A (INHBA) associated with a significantly reduced survival (Fig. 2e-g (top), hazard ratio (HR)=5.82 and $p<0.0001$ for GSE21032, HR=1.93 and $p<0.0001$ for GSE16560 and HR=7.47 and $P=0.0667$ for GSE3933). In addition, the expression of INHBA in stratified risk groups was significantly higher in the high- vs low-risk group (Fig. 2e'-g'). Oncomine (Compendia Bioscience, Waltham, MA, USA) comparison of the expression of INHBA in both primary site and metastases in 3 different data sets including Taylor MSKCC Prostate (181 samples from primary site and 37 samples from metastases), Chandran Prostate (10 samples from primary site and 21 from metastases) and Ramaswamy Prostate (10 from primary site and 3 from metastases), showed enhanced Activin A expression in metastases when compared with the corresponding primary site (Fig. 2h). On the other hand, TGF-β1, TGF-βII and TGF-βIII showed no significant upregulation in metastasis whereas Nodal exerted similar pattern as Activin A (data not shown). Overall, our analysis of the clinical data sets implied that high expression of Activin/Nodal ligands correlates with a poor prognosis and metastasis in prostate cancer patients.

Activin signaling controls the size of ALDH^{hi} subpopulation, clonogenicity, proliferation and invasion through ERK1/2 and SMad2/3-Smad4 signaling

Next, we unraveled the role of Activin signaling in prostate cancer aggressiveness. PC-3M-Pro4 and C4-2B were stimulated with Activin A, which induced phosphorylation of Smad2 and ERK1/2 (Fig. 3a, 3b). This Smad2 phosphorylation was suppressed by treatments of ALK inhibitors SB431542 and SB505124[44]. The treatment of SB505124 also inhibited Activin A induced ERK1/2 phosphorylation. To further confirm if SB505124 inhibits ERK1/2 through targeting Activin A signaling rather than directly targeting ERK1/2, we treated PC-3M-Pro4 with Follistatin, a Activin A antagonist[45]. In consistence with SB505124, the treatment with follistatin reduced Activin A-induced ERK1/2 phosphorylation (Fig. S2). This result indicated that SB505124 is stronger than SB431542 in Activin signaling inhibition (Fig. 3a, 3b). Next the effects of the treatments on cell proliferation were assessed. Although neither Activin A stimulation nor co-treatment with SB431542 displayed a significant effect on cell proliferation,

SB505124 significantly inhibited cell growth by 70% within 72hours in both PC-3M-Pro4 (Fig. 3c) and C4-2B (Fig. 3d). We next measured the self-renewal ability of the cancer cells by performing clonogenicity assay. Surprisingly, both SB505124 and SB431542 efficiently blocked the clonogenicity after 14 days of culture (Fig. 3e). In addition, we observed that the ratio ALDH^{hi} subpopulation in PC-3M-Pro4 was significantly inhibited by SB431542 after 4 days treatment (Fig. 3f, Fig. S3a), implying Activin A drives the CSC-like phenotype through Smad2 signaling.

We next confirmed if Smad2 signaling drove the CSC-like phenotype and the metastatic potential of the cancer cells. Given that phosphorylated Smad2/3 regulates expression of downstream genes through binding to and activating Smad4, we therefore introduced SMAD4 knockdown in PC-3M-Pro4 to detected how the activation of Smad2/3-Smad4 pathway affected CSC-like phenotype and metastatic capacity of the cancer cells (Fig. S4 a-c). As we expected, the knockdowns of SMAD4 significantly inhibited the size of ALDH^{hi} CSC-like subpopulation. Importantly, both SMAD4 knockdowns significantly inhibited clonogenecity *in vitro* and metastatic tumor initiation in zebrafish xenografts, indicating indeed Activin A promotes PCa cancer CSC-like phenotype and metastatic tumorigenecity through Smad2/3-Smad4 signaling.

Considering SB505124 suppressed cell proliferation associated with an inhibition of ERK1/2 phosphorylation, we also determined whether Activin A regulated cell division by ERK signaling. Western blot of treated PC-3M-Pro4 with ERK1/2 specific inhibitor SCH772984, showed that 5uM SCH772984 was sufficient to decrease ERK1/2 phosphorylation (Fig. 3g). In WST assays, the SCH772984 treatment significantly inhibited the cell proliferation without impairing the size of ALDH^{hi} subpopulation (Fig. 3h). Taken together the data suggests that Activin A regulates PCa cell proliferation via activation of ERK signaling while governs stem-like phenotypes via activation of Smad2 signaling.

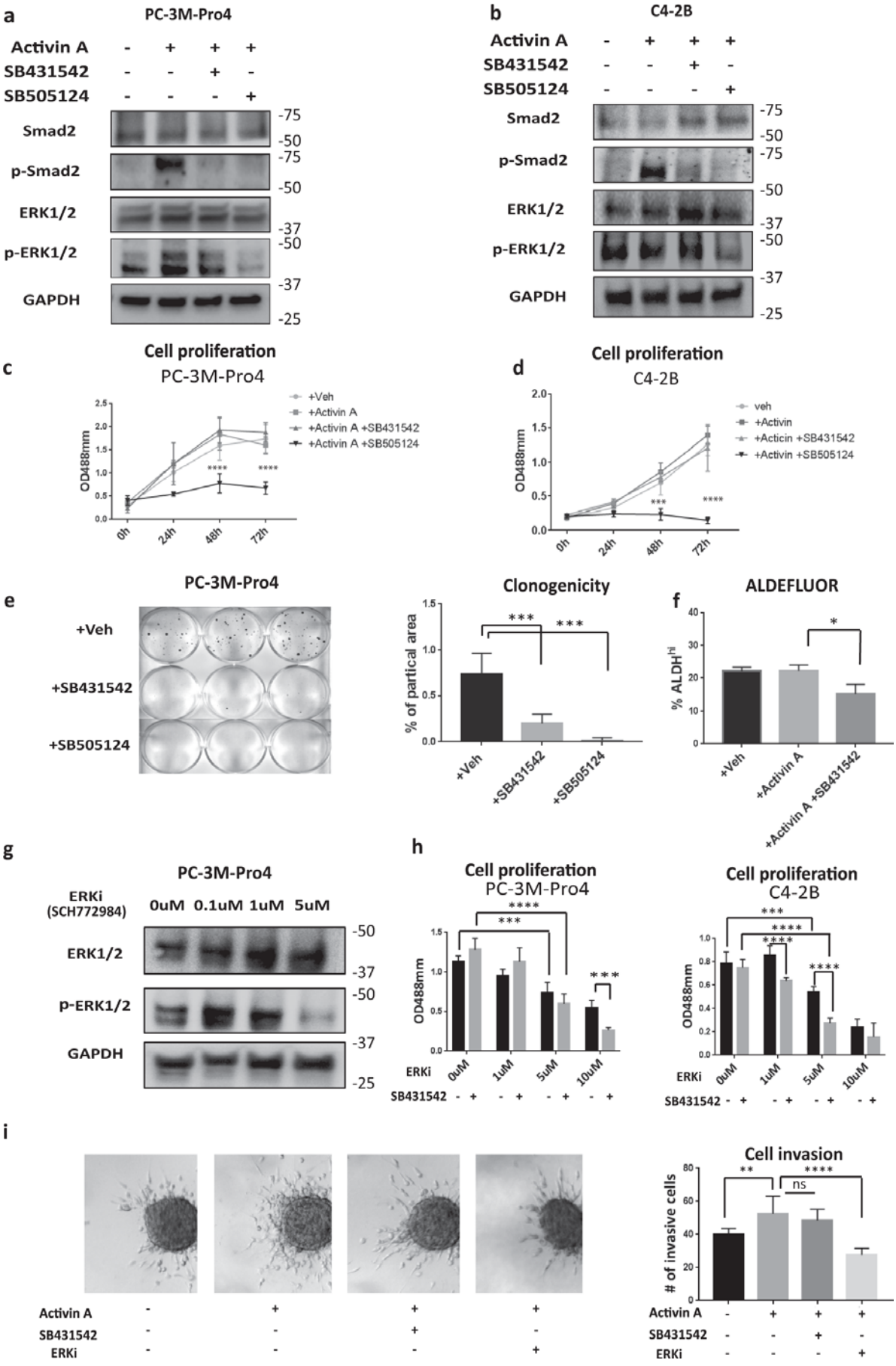
a
PC-3M-Pro4
Activin A - + + +
SB431542 - - + -
SB505124 - - - +
Smad2
p-Smad2
ERK1/2
p-ERK1/2
GAPDH
-75
-50
-75
-50
-37
-50
-37
-25
b
C4-2B
Activin A - + + +
SB431542 - - + -
SB505124 - - - +
Smad2
p-Smad2
ERK1/2
p-ERK1/2
GAPDH
-75
-50
-75
-50
-37
-50
-37
-25
c
Cell proliferation
PC-3M-Pro4
OD488mm
+Veh
+Activin A
+Activin A +SB431542
+Activin A +SB505124
0h
24h
48h
72h
d
Cell proliferation
C4-2B
OD488mm
veh
+Activin
+Acticin +SB431542
+Activin +SB505124
0h
24h
48h
72h
e
PC-3M-Pro4
+Veh
+SB431542
+SB505124
Clonogenicity
% of partical area
+Veh
+SB431542
+SB505124
f
ALDEFLUOR
% ALDH^hi
+Veh
+Activin A
+Activin A +SB431542
g
PC-3M-Pro4
ERKi (SCH772984)
0uM 0.1uM 1uM 5uM
ERK1/2
p-ERK1/2
GAPDH
-50
-37
-50
-37
-25
h
Cell proliferation
PC-3M-Pro4
OD488mm
ERKi
SB431542
0uM
1uM
5uM
10uM
Cell proliferation
C4-2B
OD488mm
ERKi
SB431542
0uM
1uM
5uM
10uM
i
Activin A - + + +
SB431542 - - + -
ERKi - - - +
Cell invasion
# of invasive cells
ns
Activin A - + + +
SB431542 - - + -
ERKi - - - +

Fig. 3 Activin A signaling controls the size of ALDH^{hi}, clonogenicity, proliferation and invasion through Smad2 and ERK1/2 signaling. (a-b) Activin A induced Smad2 phosphorylation was inhibited by SB431542 and SB505124 however Activin A induced ERK1/2 phosphorylation is only inhibited by SB505124 in PC-3M-Pro4. (b) Exogenous Activin A stimulation enhanced Smad2 phosphorylation in C4-2B and was inhibited by SB431542 and SB505124. (c-d) SB505124 but not SB431542 suppressed cell proliferation in PC-3M-Pro4 and C4-2B (n=6). (e) SB431542 and SB505124 significantly inhibited clonogenicity in PC-3M-Pro4. (f) 4 days treatment with SB431542 inhibited the size of ALDH^{hi} subpopulation in PC-3M-Pro4 (n=3). (g) Treatment with 5uM SCH772984 decreased ERK1/2 phosphorylation. (h) Targeting of ERK1/2 by SCH772984 significantly inhibited PC-3M-Pro4 and C4-2B cell proliferation within 72hours and the efficacy of treatment was increased by co-targeting Smad2 with 10uM SB431542. (n=3). (i) PC-3M-Pro4 cells were embedded in 1mg/ml type I collagen and treated with 100ug/ml Activin A, 10uM SB431542 and/or 10uM SCH772984. Activin A stimulation significantly increased the number of invading cells ($p<0.01$) but this increase was blocked by SCH772984 treatment (($p<0.0001$. (n=15)).

We further tested if co-targeting Smad2 and ERK1/2 activation more efficiently inhibited cell growth. Indeed, combination of 10 μM SB431542 with 10 μM SCH772984 significantly increased the anti-proliferation effect of SCH772984 at 10μM in PC-3M-Pro4 and C4-2B (Fig. 3h), indicating co-targeting of both ERK1/2 and Smad2 signaling is a more efficient way to inhibit PCa cell growth.

In the end we detected if Activin signaling controls PCa cell invasion. PC-3M-Pro4 tumorspheroids were embedded in type I collagen. Stimulation of Activin A significantly enhanced the number of invading cells from the central mass within 3 days (Fig. 3i). This invasive phenotype was significantly inhibited by SCH772984 but not SB431542 (Fig. 3i), indicating Activin A drives cell invasion through ERK signaling.

Activin A (INHBA) knockdown suppresses the size of ALDH^{hi} subpopulation, clonogenicity, proliferation and invasion

To conform the pharmacological data, we further investigated the function of Activin A signaling by RNAi interference approach in PC-3M-Pro4 and C4-2B cells. The efficiency of the knockdowns was validated by western blot (Fig.4a). The total protein level of Activin A was suppressed by both Activin A knockdowns. The INHBAkd1, which displayed a stronger effect (90% inhibition), also blocked the phosphorylation of both Smad2 and ERK1/2, indicating the basal level of Activin A was required to sustain activation of downstream signaling (Fig.4a). Next, we performed an ALDEFLUOR assay to check if endogenous Activin A controls ALDH^{hi} subpopulation. INHBA knockdown significantly suppressed the size of ALDH^{hi} subpopulation in PC-3M-Pro4 and this inhibition was rescued by co-treatment with exogenous Activin A (Fig.4c, Fig. S3b). INHBA knockdown also reduced the expression of stemness gene NANOG (Fig. 4b). In WST and clonogenicity assays, the knockdown of INHBA significantly suppressed cell clonogenicity and proliferation in PC-3M-Pro4 and C4-2B (Fig. 4d-4g). In 3D invasion, cell invasion was significantly suppressed by INHBA kd1 and this inhibition was rescued by exogenous Activin A stimulation (Fig. 4h).

Taken together, our knockdown studies showed that the endogenous Activin A expression plays an important role in driving PCa cell aggressiveness through governing Smad2 and ERK1/2 signaling as initially determined by pharmacological approach.

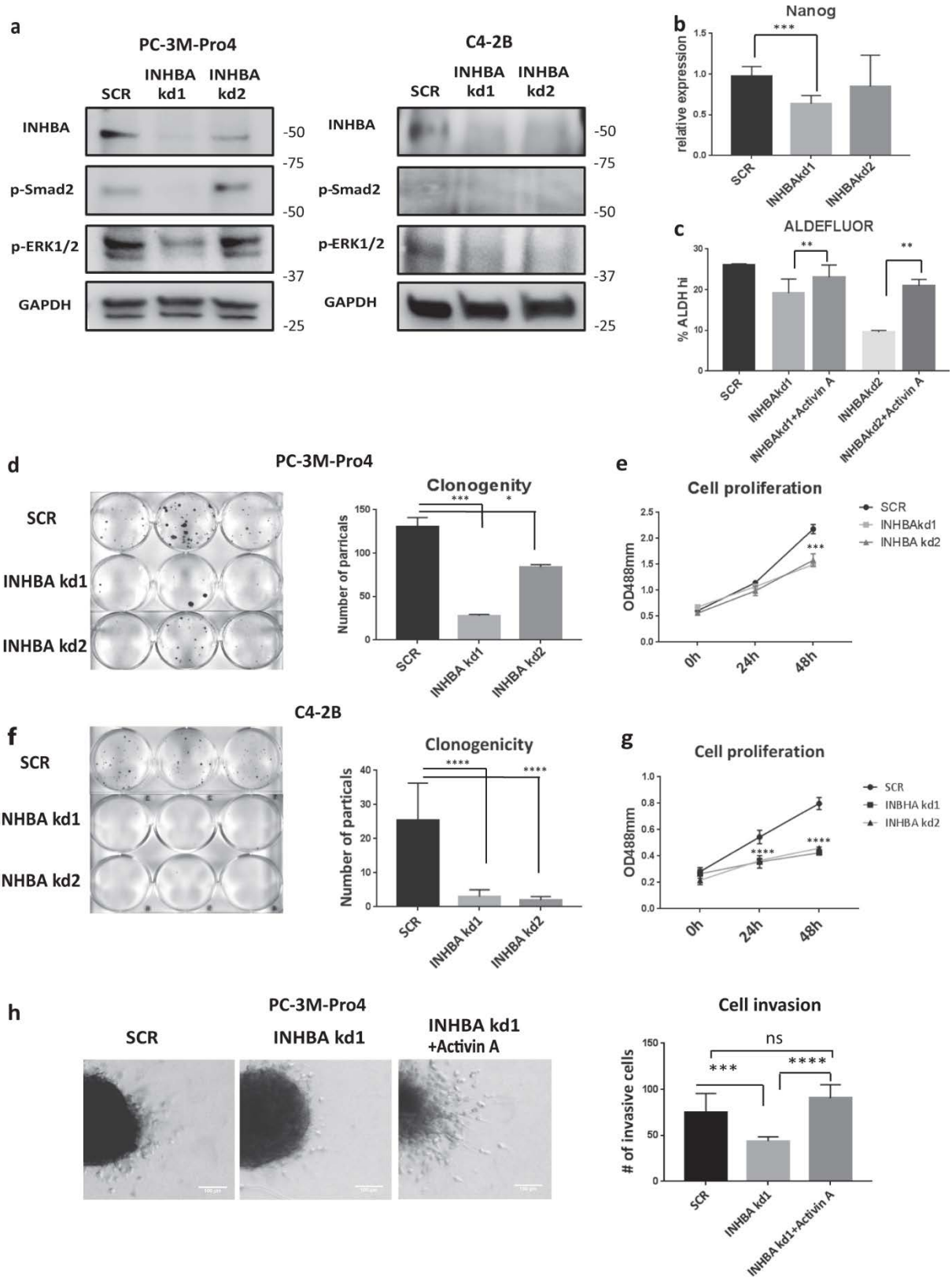

Fig. 4 Activin A (INHBA) knockdown inhibits the size of ALDH^{hi}, clonogenicity, proliferation and invasion. (a) Activin A (INHBA) knockdown in PC-3M-Pro4 and C4-2B was validated by Western blot. Two different knockdowns were used and INHBAkd1 displayed the strongest inhibition. Accordingly, Smad2 and ERK1/2 phosphorylation were strongly downregulated by kd 1 in PC-3M-Pro4 and by kd1 and kd2 in C4-2B. (b) NANOG mRNA level was significantly inhibited by INHBAkd1 ($p<0.001$, n=3). (c) Both INHBAkd1 and INHBAkd2 significantly inhibited ALDH^{hi} subpopulation size and this inhibition was rescued by 100ng recombinant Activin A (n=3, $p<0.05$). (d-g) Clonogenicity and proliferation of PC-3M-Pro4 and C4-2B were significantly inhibited by INHBAkd1 and INHBAkd2 (n=3, $p<0.05$). (h) INHBAkd1 significantly suppressed TNFα-induced cell invasion in PC-3M-Pro4. This inhibition was rescued by 100ng/ml exogenous recombinant Activin A stimulation (n=10, $p<0.05$).

Activin A (INHBA) knockdown inhibits metastatic potential of prostate cancer in ZF and mice xenografts

We assessed next if the endogenous Activin A expression is required for metastatic growth in zebrafish and mice models. We intravenously transplanted PC-3M-Pro4 containing the non-targeted control (SCR), INHBAkd1 and INHBAkd2 into ZF embryos. The metastatic growth at CHT area was significantly reduced at 4 and 6 dpi upon engraftment of the INHBAkd1 and 2 cells (Fig. 5a and 5b). Given that ALDH^{hi} cells displayed enhanced metastatic potential in both ZF and mice[3] (Fig. 5c), we tested if targeting endogenous Activin A could impair the metastatic potential of the ALDH^{hi} cells. We sorted both ALDH^{hi} and ALDH^{low} cells from the bulk population of either SCR control or the INHBA kd cells and transplanted them into ZF. Consequently, the ALDH^{hi} cells from SCR control induced the strongest metastatic growth in CHT (Fig. 5c and 5d). The ALDH^{hi} cells from INHBAkd1, however, displayed a reduced metastatic growth and had no significant difference with the ALDH^{low} INHBAkd1 (Fig. 5c and 5d), indicating endogenous Activin A expression controls the metastatic potential of PCa CSCs.

We next injected in the mice tibia PC-3M-Pro4 Luc2 SCR and PC-3M-Pro4 Luc2 INHBAkd1. The outgrowth and osteolytic ability of the prostate cancer cells in mice bone was respectively assessed by BLI signal and X-ray imaging. The SCR control cells generated advanced osteolytic lesion associated with strong tumor growth whereas the INHBAkd cells resulted in significantly reduced cancer burden and smaller osteolytic bone lesion ((Fig. 5e-5g, Supplementary Fig. S5b).

Altogether, our *in vivo* studies in ZF and mice underscored the critical role of Activin A in PCa bone metastasis.

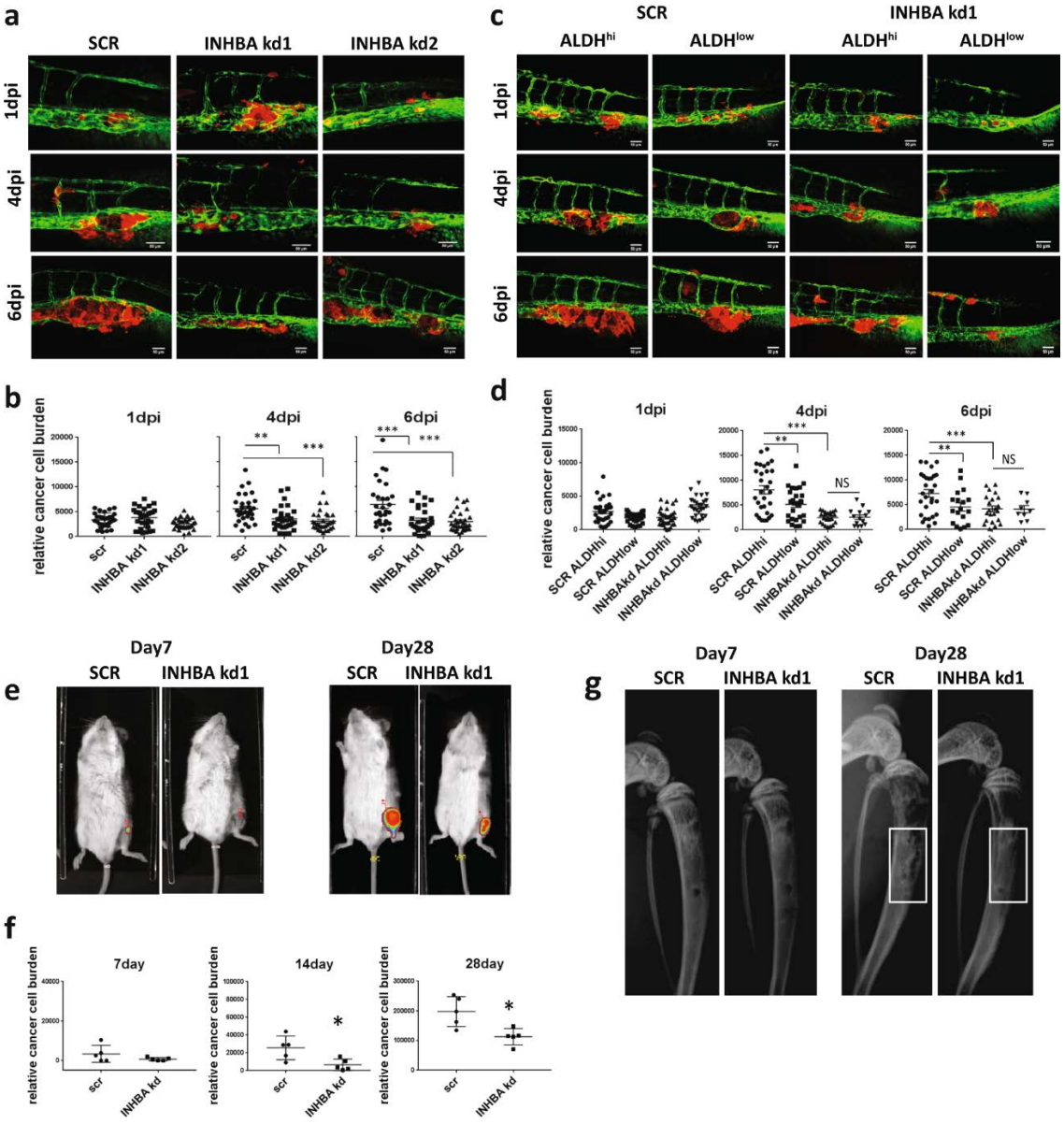

Fig. 5 Activin A (INHBA) knockdown impairs metastatic potential of prostate cancer cells *in vivo*. (a-b) INHBAkd1 significantly inhibited metastatic growth of PC-3M-Pro4 in ZF xenograft (n=60, p<0.001). (c-d) ALDH^{hi} and ALDH^{low} subpopulation were respectively sorted from PC-3M-Pro4-mCherry-SCR and PC-3M-Pro4-mCherry-INHBAkd1. After injection, ALDH^{hi} SCR showed the strongest metastatic phenotype but the ALDH^{hi} with INHBAkd1 displayed significantly reduced metastatic tumor growth at 4 and 6 dpi (p<0.01, n=25-30). Scale bar=50um. (e) PC-3M-Pro4-Luc2-SCR and PC-3M-Pro4-Luc2-INHBAkd1 were injected into tibia of CB17 SCID mice. Tumor growth was monitored by bioluminescent imaging (BLI) after 7, 14 and 28 days. (f) In the graphs total BLI units were reported as a measure of tumor burden growth. The INHBAkd significantly inhibited cell growth at day 14 and day 28 (n=5, p<0.05). (h) INHBAkd1 strongly impaired the progression of osteolytic lesions induced by PC-3M-Pro4-Luc2 cells.

The expression of Activin A is regulated by NF-κB activation

Finally, we investigated how Activin A is regulated by the microenvironment during metastasis. Given that the expression of Activin A was increased together with an upregulation of NF-κB associated cytokines in both ZF and mice xenografts (Fig. 1g-1h, Fig. 2c), we hypothesize a close correlation between NF-κB activation and Activin A production. By whole

mount immunofluorescence, nuclear phosphorylated P65 (a marker of activated NF-κB), endogenous Activin A and phosphorylated Smad2 were detected in PC-3M-Pro4 cells after colonizing the CHT (Fig. 6a). To further validate the relevance between NF-κB activation and Activin A expression, we treated the cancer cells with recombinant human TNFα (known NF-κB activator) for 48 hours. As we expected, this stimulation induced an upregulation of Activin A protein level (Fig. 6a, 6b) accompanied by enhanced P65 phosphorylation (Fig. 6b), and pro-inflammatory cytokines GM-CSF, IL-8 and CCL2 expression (Fig. 6d, Fig.s6), respectively. The TNFα stimulation also significantly promoted the expression of Activin A yielding a 4-fold increase in PC-3 and a 16-fold increase in PC-3M-Pro4 (Supplementary Fig. S6a). Collectively, this data indicated that activation of NF-κB is a key driver of Activin A expression. To further prove if this TNFα-induced Activin A upregulation is NF-κB dependent, we co-treated the cancer cells with TNFα and NF-κB inhibitor, (IKK inhibitor NF-κB Activation Inhibitor IV). The expression of TNFα-dependent pro-inflammatory factors and Activin A was suppressed by 50% in PC-3M-Pro4 (Fig. 6d). We also stimulated the cells with recombinant GM-CSF, CCL2 and IL8 to test if the pro-inflammatory cytokines found upregulated in NGS data and by NF-κB activation *in vitro* could regulate Activin A expression. Exclusive stimulation with 10ng/ml IL-8 for 48 hours significantly increased the expression of CCL2, GM-CSF and Activin A (Fig. 6e) implicating the Acitivin A expression was mainly controlled by NF-κB-IL8 axis.

Next, we tested if this NF-κB dependent Activin A expression was sufficient to activate Activin/Nodal signaling pathway. We stimulated PC-3M-Pro4 with recombinant human TNFα, Activin A and/or TGF-β (as positive control) for 48 hours in low serum medium and measured the phosphorylation of Smad2 and ERK1/2 with phospho-specific antibodies. Stimulation with either Activin A or TGF-β enhanced phosphorylation of Smad2 and ERK1/2. Importantly, the TNFα treatment increased Smad2 phosphorylation (Fig. 6c), indicating that NF-κB activation can directly control Activin signaling.

To test if the NF-κB-induced Activin expression was sufficient to drive the invasive phenotype of the PCa cells, we performed 3D invasion assay. The stimulation of 10 ng/ml TNFα significantly enhanced cell invasion. This TNFα-induced cell invasion was significantly inhibited by INHBA kd, indicating TNFα promoted cell invasion through the induction of Activin signaling pathway. (n=8-10) (Fig. 6f).

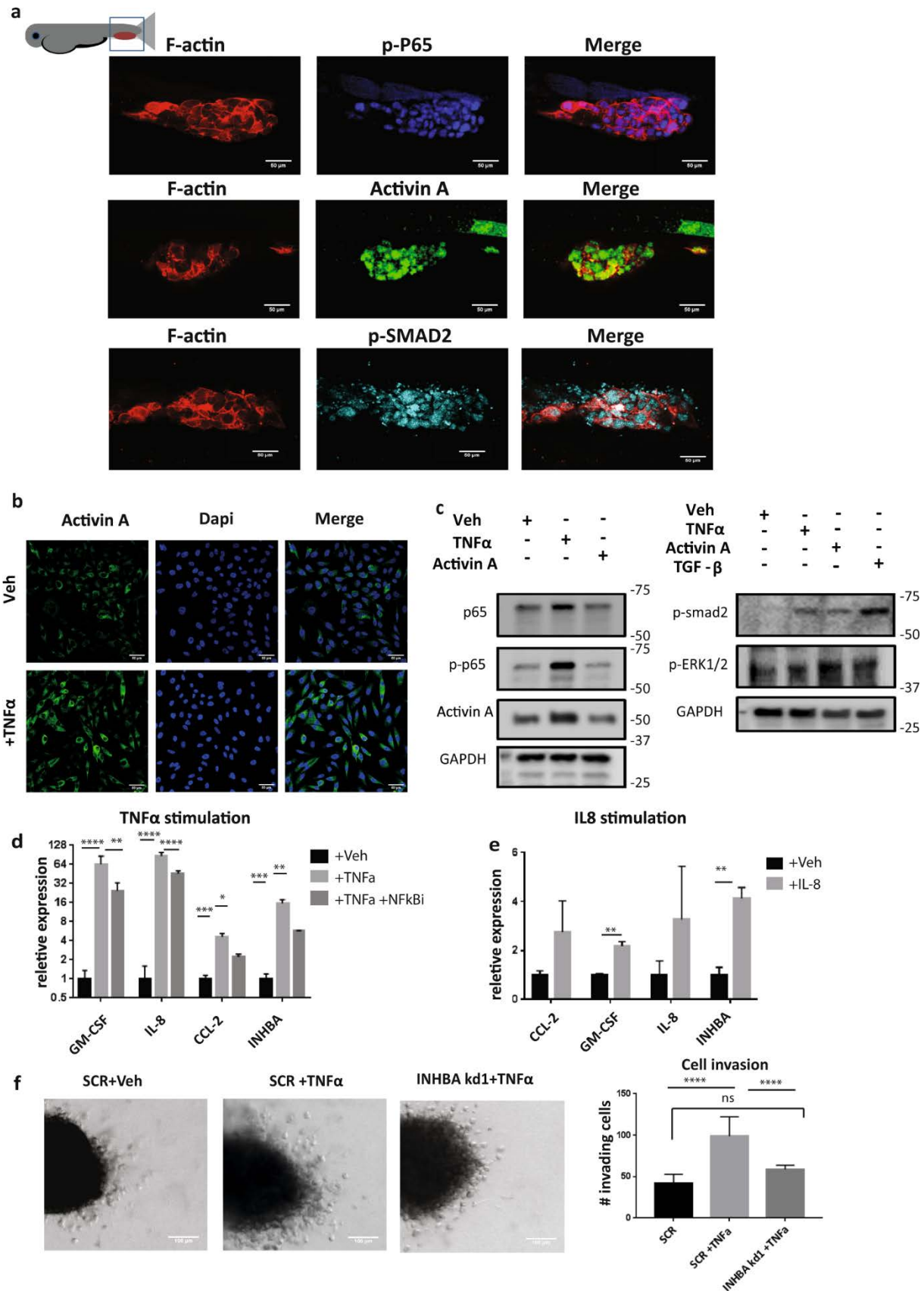

Fig. 6 Activin A (INHBA) expression is regulated by NF-κB activation. (a) Whole mount immunofluorescence was performed on the metastases formed by PC-3M-Pro4 at CHT area at 6dpi. Nuclear phosphorylated-P65 (blue), Activin A (green) and nuclear phosphorylated-Smad2 (cyan) were detected in the tumor cells labeled with lifeact-mCherry (red), scale bar=50um. (b) PC-3M-Pro4 were treated with vehicle control, 10ng/ml human recombinant

TNFα, 100ng/ml Activin A and/or 10ng/ml TGFβ for 48hours. The treatment with TNFα increases P65 phosphorylation and Activin A expression (left and middle panel). TNFα, Activin A and TGF-β treatments induced Smad2 phosphorylation but Activin A specifically increased ERK1/2 phosphorylation (right panel). (c) PC-3M-Pro4 were treated with either 10ng TNFα or 10ng TNFα + 4uM NF-κB Activation Inhibitor IV. qPCR showed that TNFα treatment upregulated pro-inflammatory cytokines and INHBA and this upregulation was inhibited by NF-κB Activation Inhibitor IV in PC-3M-Pro4 cells (n=3, $p<0.05$). (d) Human recombinant IL-8 (10ng) treatment of PC-3M-Pro4 induced expression of pro-inflammatory factors and Activin A (INHBA) (n=3, $p<0.01$). (E) PC-3M-Pro4 bearing either SCR or INHBA kd1 were embedded in 1mg/ml type I collagen (1000cells/sphere) and treated with either Veh control or TNFα. The number of cells invading from central mass were counted. (n=>8).

Discussion

The metastatic cascade is a highly complex and inefficient process, subject to regulation by host microenvironment. Combining zebrafish and mice xenografts, we dissected an essential role of microenvironment induced endogenous Activin A expression in driving PCa metastasis. This result is in line with our analysis of clinical datasets, which shows Activin A expression as being elevated in metastases and correlating with poor prognosis, in a stratified high-risk patient cohort (Fig. 2).

We firstly traced metastatic behavior of human PCa cells in zebrafish xenograft and detected how PCa cells responded to the microenvironment during metastatic growth. Zebrafish genome shares similarity to human genome as 70% of human genes are found in ZF and the availability of optically transparent strains facilitates real-time and longitudinal studies of cancers in an intact microenvironment[46,47,48,49]. It has been already proved that molecular and cellular cues existing in the zebrafish microenvironment can drive the metastatic behavior of human cancer cells [43,50]. In addition, the zebrafish provides the unique opportunity to study the key initial steps of metastasis onset in great details by easily combining high resolution imaging and transcriptomic analysis[51,52,53]. We observed that in ZF, the I.V. transplantation of osteotropic cancer cell line PC-3M-Pro4 resulted in strong metastatic tumor growth. Transcriptional comparison of PC-3M-Pro4 cultured vs micro-dissected tissue samples derived from zebrafish xenograft tissue, revealed that cancer cells isolated from zebrafish lesions displayed a stem-like/EMT phenotype after homing to the zebrafish hematopoietic tissue. This is consistent with previous studies in mice models, in which the size of CSC subpopulation was increased when osteotropic prostate cancer cells colonized the mouse bone hematopoietic niche[41,42]. They further indicated that this colonization was SDF-1-CXCR4 axis dependent. Recently, our group demonstrated that human triple-negative breast cancer cells colonized the zebrafish hematopoietic niche by sensing host SDF-1[50]. Attenuation of either SDF1 in zebrafish or CXCR4 receptor in these cells significantly suppressed the metastatic onset. Therefore, we hypothesized that the metastatic behavior of osteotropic PCa cells in the zebrafish hematopoietic niche, at least to a certain extent, is comparable with their behavior in mice.

In agreement with this, we observed an upregulation of stemness genes, NF-κB-dependent cytokines and Activin genes in the prostate cancer cells when they metastasized in both zebrafish and mice (Fig. 1 and Fig. 2). The *in vitro* activation of NF-κB through stimulation with

TNFα and IL-8 led to pro-inflammatory cytokines and Activin A over-expression suggesting that NF-κB dependent cytokines control Activin A expression (Fig. 6b-d). This finding is in line with a recent study, showing that the cytokine-dependent NF-κB activation could promote mesenchymal features of CSCs through regulating Activin A expression in Non-Small Cell Lung Cancer[22]. Therefore, we addressed the link between endogenous Activin A expression and CSCs regulation in prostate cancer progression. Our data showed that Activin A sustains the stem-like phenotype of the cancer cells by regulating Smad2/3-Smad4 signaling and in parallel drives cell proliferation and invasion through ERK1/2 signaling pathway (Fig. 3). Targeting of Activin signaling pathway by either Activin receptor inhibitors or INHBA shRNAs significantly suppressed Smad2 and ERK1/2 phosphorylation, proliferation, clonogenicity, invasion and the size of $ALDH^{hi}$ subpopulation in the PCa cells in culture (Fig. 3, Fig. S3 and Fig. 4). *In vivo*, Activin A knockdown significantly suppressed the tumorigenicity in zebrafish and mice xenograft (Fig. 5). Importantly, Activin A knockdown also suppressed the metastatic growth of the $ALDH^{hi}$ subpopulation, suggesting that Activin A is required for not only maintaining the size of $ALDH^{hi}$ fraction but also regulating their metastatic capacity (Fig. 5c). Notably, in our experiments, the strong INHBA kd1 had a less inhibitory effect on $ALDH^{hi}$ compared with the moderate INBHA kd2, although INHBA kd1 more sufficiently suppressed Smad2 and ERK1/2 phosphorylation, Nanog expression and clonogenecity. We hypothesized this discrepancy was due to the cellular stress induced by the strong INHBA kd1. The cellular stress may elicit ALDH activity partially compensating the inhibitory effect of $ALDH^{hi}$ by the INHBA knockdown[54].

Consistent with our results, the pro-tumor effect of activin A on malignant prostate cancer was also demonstrated by Holfland et al[55]. They found Activin A could promote cancer cell growth by stimulating local androgen production via regulating 17β-HSD in CRPCs. In contrast, it has been also shown that Activin A acts as a tumor suppressor in low grade prostate cancer cells LNCaP and DU145[23]. The high-grade cancer cells PC-3, however, were resistant to anti-proliferative effects of activin. This resistance was believed to be mediated by Activin A antagonist Follistatin and Activin C[24]. C4-2B cells are derived from mice bone metastases of C4-2, a castration-resistant subclone of LNCaP[56]. By qPCR, we measured a detectable expression of Activin A in C4-2B but not in LNCaP (Fig. S6a). This result is in line with the clinical dataset analysis indicating that higher expression of Activin A correlates with bone metastasis. Moreover, we did not see the significant anti-proliferation effect of Activin A on C4-2B (Fig. 3d) in contrast to the results obtained in LNCaP[23]. This tolerance seems to be antagonist-independent since the Activin A treatment still induced strong Smad2 phosphorylation in both PC-3M-Pro4 and C4-2B without impairing cell proliferation (Fig. 3a-3d).

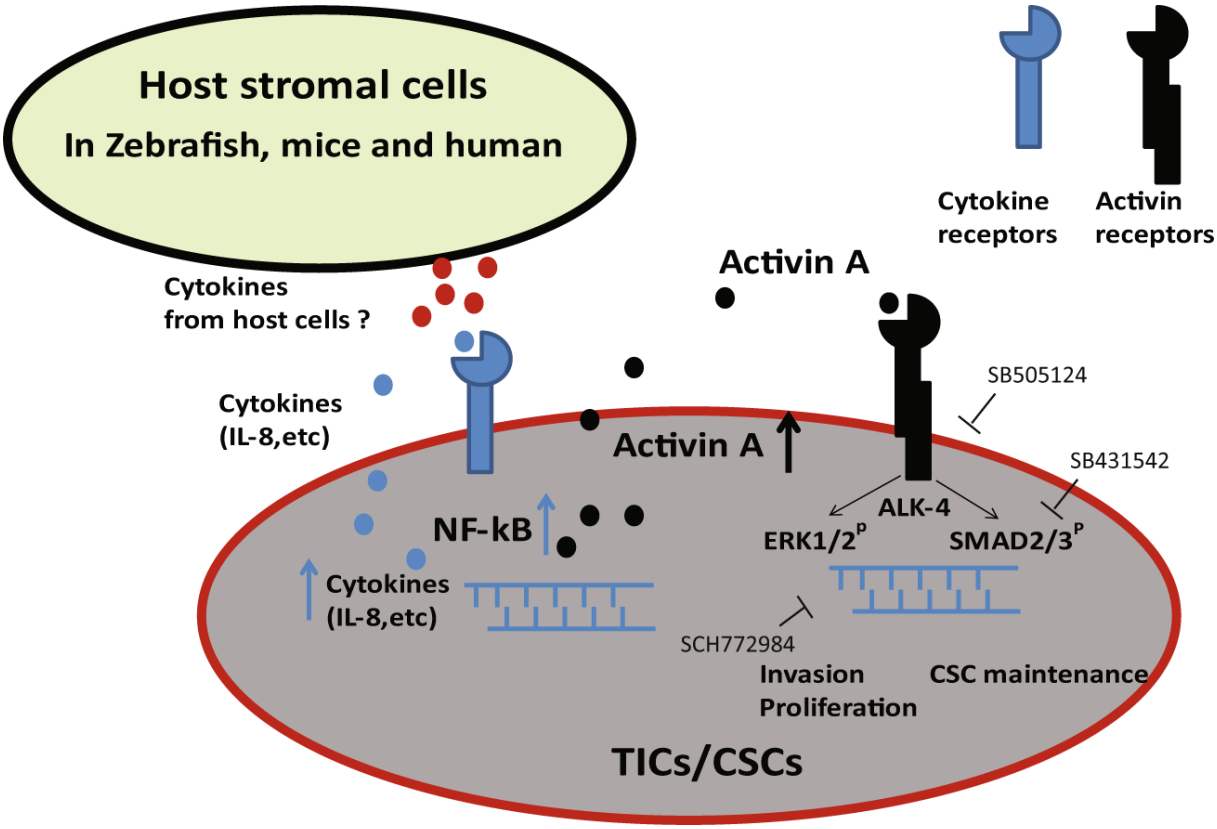

Fig. 7 Schematic representation of the proposed role of Activin signaling in prostate cancer metastasis. Following the extravasation of the ALDH^{hi} cells, cellular and molecular cues in the distant microenvironment (conserved between zebrafish, mice and human) trigger the activation of NF-κB in the cancer cells resulting in a production of pro-inflammatory cytokines and Activin A. Cytokines (like IL-8) were able to develop a positive feedback loop in the micro-environment to maintain and/or amplify the NF-κB activity. In parallel, the endogenous Activin A induced by NF-κB activation sustains the CSC-like properties and controls cell division and invasion through Smad and ERK signaling pathway. Targeting/co-targeting Activin A specific receptors and/or ERK1/2 impairs the aggressiveness of prostate cancer cells.

In order to address if cancer cells acquire an enhanced stem-like phenotype by the production of Activin A, we treated the cancer cells with either the exogenous Activin A or TNFα *in vitro*. We did not observe a significant increase of the ALDH^{hi} subpopulation (data not shown), suggesting that other factors in both zebrafish and mammalian hematopoietic niche could be needed for cell plasticity. Additionally, we have not yet determined the molecular cues driving the NF-κB activation and Activin A expression in the microenvironment. Lu et al demonstrated that monocytes and macrophages could support breast cancer stem cell niche through Ephrin-EphA4 axis-dependent NF-κB activation and cytokines induction in breast CSCs[57]. Indeed, we also visualized a recruitment of TNFα positive macrophages to the prostate cancer cells during metastasis in zebrafish (data not shown). Future studies are required to understand if this ZF TNFα from macrophage is sufficient to trigger NF-κB activation and Activin A expression, and therefore promote PCa metastasis. Moreover, additional studies are also necessary to determine if and when Activin inhibitors could be administrated to patients and to further understand at what stage Activin A-dependency in prostate cancer develops

In conclusion, for the first time in this study we show that human cancer cells display a similar response to the microenvironment in both zebrafish and mice xenograft models, induce NF-κB -dependent Activin A expression, which specifically controls the Smad2/3-Smad4 dependent CSC-like properties and ERK1/2 driven proliferation and invasion of PCa cells during metastasis (Fig. 7). Therefore, the combination of both *in vivo* models is an excellent combined platform to explore cancer cell-microenvironment interactions. Using this combined platform, we identified a pro-metastatic function of the microenvironment-dependent Activin A expression in malignant prostate cancer. This endogenous Activin A is crucial for sustaining CSCs subpopulation and regulates their metastatic capacity. Overall, our study provides evidence that Activin A could be a potent target for therapeutic intervention against late stage prostate cancer.

Acknowledgments

We thank Dr. Gabriel van der Pluijm (Deportment of Urology, LUMC) for providing experimental material, Prof. Peter ten Dijke (Department of Molecular Cell Biology) for providing experimental material and critical scientific discussion and Guido de Roo from the Flow cytometry facility (Department of Hematology, LUMC) for technical support, Prof. Rob Hoeben and Martijn Rabelink (Department of Cell Biology, LUMC) for providing lenti-viral shRNA vectors (Sigma-Aldrich). The present work was supported by a personalized medicine grant from Alpe D'HuZes (AdH)/KWF PROPER entitled “Near-patient prostate cancer models for the assessment of disease prognosis and therapy” (UL2014-7058) and SNF 31003A_169352.

Reference

[1] Jemal, A., Center, M. M., DeSantis, C., and Ward, E. M. (2010). Global patterns of cancer incidence and mortality rates and trends. *Cancer Epidemiology and Prevention Biomarkers*, 1055-9965.

[2] Collins, A. T., Berry, P. A., Hyde, C., Stower, M. J., & Maitland, N. J. (2005). Prospective identification of tumorigenic prostate cancer stem cells. *Cancer research*, *65*(23), 10946-10951.

[3] van den Hoogen, C., van der Horst, G., Cheung, H., Buijs, J. T., Lippitt, J. M., Guzmán-Ramírez, N., et al. (2010). High aldehyde dehydrogenase activity identifies tumor-initiating and metastasis-initiating cells in human prostate cancer. *Cancer research*, 0008-5472.

[4] Jones, R. J., Barber, J. P., Vala, M. S., Collector, M. I., Kaufmann, S. H., Ludeman, S. M., et al. (1995). Assessment of aldehyde dehydrogenase in viable cells. *Blood*, *85*(10), 2742-2746.

[5] Massagué, J. (2008). TGFβ in cancer. *Cell*, *134*(2), 215-230.

[6] Shi, Y., & Massagué, J. (2003). Mechanisms of TGF-β signaling from cell membrane to the nucleus. *Cell*, *113*(6), 685-700.

[7] Quail, D. F., Zhang, G., Findlay, S. D., Hess, D. A., & Postovit, L. M. (2014). Nodal promotes invasive phenotypes via a mitogen-activated protein kinase-dependent pathway. *Oncogene*, *33*(4), 461.

[8] Clements, M., Pernaute, B., Vella, F., & Rodriguez, T. A. (2011). Crosstalk between Nodal/activin and MAPK p38 signaling is essential for anterior-posterior axis specification. *Current Biology*, *21*(15), 1289-1295.
[9] James, D., Levine, A. J., Besser, D., & Hemmati-Brivanlou, A. (2005). TGFβ/activin/nodal signaling is necessary for the maintenance of pluripotency in human embryonic stem cells. *Development*, *132*(6), 1273-1282.
[10] Xiao, L., Yuan, X., & Sharkis, S. J. (2006). Activin A maintains self-renewal and regulates fibroblast growth factor, Wnt, and bone morphogenic protein pathways in human embryonic stem cells. *Stem cells*, *24*(6), 1476-1486.
[11] Schier, A. F., & Shen, M. M. (2000). Nodal signalling in vertebrate development. *Nature*, *403*(6768), 385.
[12] Nomura, M., & Li, E. (1998). Smad2 role in mesoderm formation, left–right patterning and craniofacial development. *Nature*, *393*(6687), 786.
[13] Loomans, H. A., & Andl, C. D. (2014). Intertwining of activin A and TGFβ signaling: dual roles in cancer progression and cancer cell invasion. *Cancers*, *7*(1), 70-91.
[14] Strizzi, L., Bianco, C., Normanno, N., & Salomon, D. (2005). Cripto-1: a multifunctional modulator during embryogenesis and oncogenesis. *Oncogene*, *24*(37), 5731.
[15] Gray, P. C., & Vale, W. (2012). Cripto/GRP78 modulation of the TGF-β pathway in development and oncogenesis. *FEBS letters*, *586*(14), 1836-1845.
[16] Lonardo, E., Hermann, P. C., Mueller, M. T., Huber, S., Balic, A., Miranda-Lorenzo, I., et al. (2011). Nodal/Activin signaling drives self-renewal and tumorigenicity of pancreatic cancer stem cells and provides a target for combined drug therapy. *Cell stem cell*, *9*(5), 433-446.
[17] Zoni, E., Chen, L., Karkampouna, S., Granchi, Z., Verhoef, E. I., La Manna, F., et al. (2017). CRIPTO and its signaling partner GRP78 drive the metastatic phenotype in human osteotropic prostate cancer. *Oncogene*, *36*(33), 4739.
[18] Karkampouna, S., van der Helm, D., Gray, P. C., Chen, L., Klima, I., Grosjean, J., et al. (2018). CRIPTO promotes an aggressive tumour phenotype and resistance to treatment in hepatocellular carcinoma. *The Journal of pathology*.
[19] Brown, C. W., Li, L., Houston-Hawkins, D. E., & Matzuk, M. M. (2003). Activins are critical modulators of growth and survival. *Molecular Endocrinology*, *17*(12), 2404-2417.
[20] Wang, Q., Wen, Y. G., Li, D. P., Xia, J., Zhou, C. Z., Yan, D. W., et al. (2012). Upregulated INHBA expression is associated with poor survival in gastric cancer. *Medical oncology*, *29*(1), 77-83.
[21] Bashir, M., Damineni, S., Mukherjee, G., & Kondaiah, P. (2015). Activin-A signaling promotes epithelial–mesenchymal transition, invasion, and metastatic growth of breast cancer. *NPJ breast cancer*, 1, 15007.
[22] Wamsley, J. J., Kumar, M., Allison, D. F., Clift, S. H., Holzknecht, C. M., Szymura, S. J., et al. (2014). Activin upregulation by NF-κB is required to maintain mesenchymal features of cancer stem-like cells in non-small cell lung cancer. *Cancer research*, canres-2702.
[23] Dalkin, A. C., Gilrain, J. T., Bradshaw, D., & Myers, C. E. (1996). Activin inhibition of prostate cancer cell growth: selective actions on androgen-responsive LNCaP cells. *Endocrinology*, *137*(12), 5230-5235.
[24] Gold, E., & Risbridger, G. (2012). Activins and activin antagonists in the prostate and prostate cancer. *Molecular and cellular endocrinology*, *359*(1-2), 107-112.
[25] McKenzie, S., & Kyprianou, N. (2006). Apoptosis evasion: the role of survival pathways in prostate cancer progression and therapeutic resistance. *Journal of cellular biochemistry*, *97*(1), 18-32.

[26] Leto, G., Incorvaia, L., Badalamenti, G., Tumminello, F. M., Gebbia, N., Flandina, C., et al. (2006). Activin A circulating levels in patients with bone metastasis from breast or prostate cancer. *Clinical & experimental metastasis*, *23*(2), 117-122.
[27] Aguirre-Gamboa, R., Gomez-Rueda, H., Martínez-Ledesma, E., Martínez-Torteya, A., Chacolla-Huaringa, R., Rodriguez-Barrientos, A., et al. SurvExpress: an online biomarker validation tool and database for cancer gene expression data using survival analysis. *PloS one*, *8*(9), e74250.
[28] Lawson, N. D., & Weinstein, B. M. (2002). In vivo imaging of embryonic vascular development using transgenic zebrafish. *Developmental biology*, *248*(2), 307-318.
[29] Ellett, F., Pase, L., Hayman, J. W., Andrianopoulos, A., & Lieschke, G. J. (2010). mpeg1 promoter transgenes direct macrophage-lineage expression in zebrafish. *Blood*, blood-2010.
[30] Cui, C., Benard, E. L., Kanwal, Z., Stockhammer, O. W., van der Vaart, M., Zakrzewska, A., et al. (2011). Infectious disease modeling and innate immune function in zebrafish embryos. In *Methods in cell biology* (Vol. 105, pp. 273-308). Academic Press.
[31] Trapnell, C., Pachter, L., & Salzberg, S. L. (2009). TopHat: discovering splice junctions with RNA-Seq. *Bioinformatics*, *25*(9), 1105-1111.
[32] Li, H., Handsaker, B., Wysoker, A., Fennell, T., Ruan, J., Homer, N., et al. (2009). The sequence alignment/map format and SAMtools. *Bioinformatics*, *25*(16), 2078-2079.
[33] Anders, S., Pyl, P. T., & Huber, W. (2015). HTSeq—a Python framework to work with high-throughput sequencing data. *Bioinformatics*, *31*(2), 166-169.
[34] Anders, S., & Huber, W. (2010). Differential expression analysis for sequence count data. *Genome biology*, *11*(10), R106

[35] Dai, J., Hensel, J., Wang, N., Kruithof-de Julio, M., & Shiozawa, Y. (2016). Mouse models for studying prostate cancer bone metastasis. *BoneKEy reports*, *5*.
[36] Tamplin, O. J., Durand, E. M., Carr, L. A., Childs, S. J., Hagedorn, E. J., Li, P., et al. (2015). Hematopoietic stem cell arrival triggers dynamic remodeling of the perivascular niche. *Cell*, *160*(1), 241-252.
[37] Jin, H., Xu, J., & Wen, Z. (2007). Migratory path of definitive hematopoietic stem/progenitor cells during zebrafish development. *Blood*, *109*(12), 5208-5214.
[38] He, S., Lamers, G. E., Beenakker, J. W. M., Cui, C., Ghotra, V. P., Danen, E. H., et al. (2012). Neutrophil-mediated experimental metastasis is enhanced by VEGFR inhibition in a zebrafish xenograft model. The Journal of pathology, 227(4), 431-445.
[39] Drabsch, Y., He, S., Zhang, L., Snaar-Jagalska, B. E., & ten Dijke, P. (2013). Transforming growth factor-β signalling controls human breast cancer metastasis in a zebrafish xenograft model. *Breast cancer research*, *15*(6), R106.
[40] Shiozawa, Y., Pedersen, E. A., Havens, A. M., Jung, Y., Mishra, A., Joseph, J., et al. (2011). Human prostate cancer metastases target the hematopoietic stem cell niche to establish footholds in mouse bone marrow. *The Journal of clinical investigation*, *121*(4), 1298-1312.
[41] Shiozawa, Y., Berry, J. E., Eber, M. R., Jung, Y., Yumoto, K., Cackowski, F. C., et al. (2016). The marrow niche controls the cancer stem cell phenotype of disseminated prostate cancer. *Oncotarget*, *7*(27), 41217.
[42] Sacco, A., Roccaro, A. M., Ma, D., Shi, J., Mishima, Y., Moschetta, M., et al. (2016). Cancer cell dissemination and homing to the bone marrow in a zebrafish model. *Cancer research*.
[43] Hsu, W. K., Virk, M. S., Feeley, B. T., Stout, D. B., Chatziioannou, A. F., & Lieberman, J. R. (2008). Characterization of osteolytic, osteoblastic, and mixed lesions in a prostate cancer mouse model using 18F-FDG and 18F-fluoride PET/CT. *Journal of nuclear medicine: official publication, Society of Nuclear Medicine*, *49*(3), 414.

[44] Byfield, S. D., Major, C., Laping, N. J., & Roberts, A. B. (2004). SB-505124 is a selective inhibitor of transforming growth factor-β type I receptors ALK4, ALK5, and ALK7. *Molecular pharmacology*, *65*(3), 744-752.
[45] Hemmati-Brivanlou, A., Kelly, O. G., & Melton, D. A. (1994). Follistatin, an antagonist of activin, is expressed in the Spemann organizer and displays direct neuralizing activity. *Cell*, *77*(2), 283-295.

[46] Postlethwait, J. H., Yan, Y. L., Gates, M. A., Horne, S., Amores, A., Brownlie, A., et al. (1998). Vertebrate genome evolution and the zebrafish gene map. *Nature genetics*, *18*(4), 345.
[47] Zon, L. I., & Peterson, R. T. (2005). *In vivo* drug discovery in the zebrafish. *Nature reviews Drug discovery*, *4*(1), 35.
[48] Dooley, K., & Zon, L. I. (2000). Zebrafish: a model system for the study of human disease. *Current opinion in genetics & development*, *10*(3), 252-256.
[49] White, R., Rose, K., & Zon, L. (2013). Zebrafish cancer: the state of the art and the path forward. *Nature reviews Cancer*, *13*(9), 624.
[50] Tulotta, C., Stefanescu, C., Beletkaia, E., Bussmann, J., Tarbashevich, K., Schmidt, T., & Snaar-Jagalska, B. E. (2016). Inhibition of signaling between human CXCR4 and zebrafish ligands by the small molecule IT1t impairs the formation of triple-negative breast cancer early metastases in a zebrafish xenograft model. *Disease models & mechanisms*, *9*(2), 141-153.
[51] Chen, L., Groenewoud, A., Tulotta, C., Zoni, E., Kruithof-de Julio, M., van der Horst, G., et al. (2017). A zebrafish xenograft model for studying human cancer stem cells in distant metastasis and therapy response. In *Methods in cell biology* (Vol. 138, pp. 471-496). Academic Press.
[52] Fior, R., Póvoa, V., Mendes, R. V., Carvalho, T., Gomes, A., Figueiredo, N., & Ferreira, M. G. (2017). Single-cell functional and chemosensitive profiling of combinatorial colorectal therapy in zebrafish xenografts. *Proceedings of the National Academy of Sciences*, *114*(39), E8234-E8243.
[53] Liu, T. L., Upadhyayula, S., Milkie, D. E., Singh, V., Wang, K., Swinburne, I. A., et al. (2018). Observing the cell in its native state: Imaging subcellular dynamics in multicellular organisms. *Science*, *360*(6386), eaaq1392.
[54] Singh, S., Brocker, C., Koppaka, V., Chen, Y., Jackson, B. C., Matsumoto, A., et al. (2013). Aldehyde dehydrogenases in cellular responses to oxidative/electrophilicstress. *Free radical biology and medicine*, *56*, 89-101.
[55] Hofland, J., van Weerden, W. M., Steenbergen, J., Dits, N. F., Jenster, G., & de Jong, F. H. (2012). Activin A stimulates AKR1C3 expression and growth in human prostate cancer. *Endocrinology*, *153*(12), 5726-5734.
[56] Thalmann, G. N., Anezinis, P. E., Chang, S. M., Zhau, H. E., Kim, E. E., Hopwood, V. L., et al. (1994). Androgen-independent cancer progression and bone metastasis in the LNCaP model of human prostate cancer. *Cancer research*, 54(10), 2577-2581.
[57] Lu, H., Clauser, K. R., Tam, W. L., Fröse, J., Ye, X., Eaton, E. N., et al. (2014). A breast cancer stem cell niche supported by juxtacrine signalling from monocytes and macrophages. *Nature cell biology*, 16(11), 1105.

Table. S1

Cell behavior after zebrafish transplantation at 4dpi			
Cell line	Localized tumor growth	Engiogenesis	Metastaticgrowth
DU-145	+-	-	-
LNCaP	-	-	-
C4-2B	-	-	-
PC-3	+	+	+
PC-3M-Pro4	++	-	++

Suppl. Table 1. Cell behavior after zebrafish transplantation. PCa cells including DU-145, LNCaP, C4-2B, PC-3 and PC-3M-Pro4 were transplanted into Duct of Cuvier of zebrafish at 2dpi. Localized tumor growth, engiogenesis and metastasis at CHT were compared at 4dpi. PC-3M-Pro4 displayed strongest localized and metastatic tumor growth but the low grade cancer cells including DU-145, LNCap and C4-2B failed to facilite cancer progression.

Table. S2

TGF-β family members regulated in zebrafish metastasis		
Gene Symble	Fold Change	p-adjust
INHBA	14.0173351	0.009502
INHBB	Non -detected	#
INHBC	7.972730174	0.064617
Follistatin	0.247112903	1.75E-21
TGF-β1	0.420676381	0.000474
TGF-β2	0.151945486	3.35E-10
TGF-β3	0.449540544	0.056271
Nodal	6.305691745	1

Suppl. Table 2. Comparison of selected TGF-β family members expression between PC-3M- Pro4 in ZF metastasis and in culture from NGS data.

Supplementary Figures

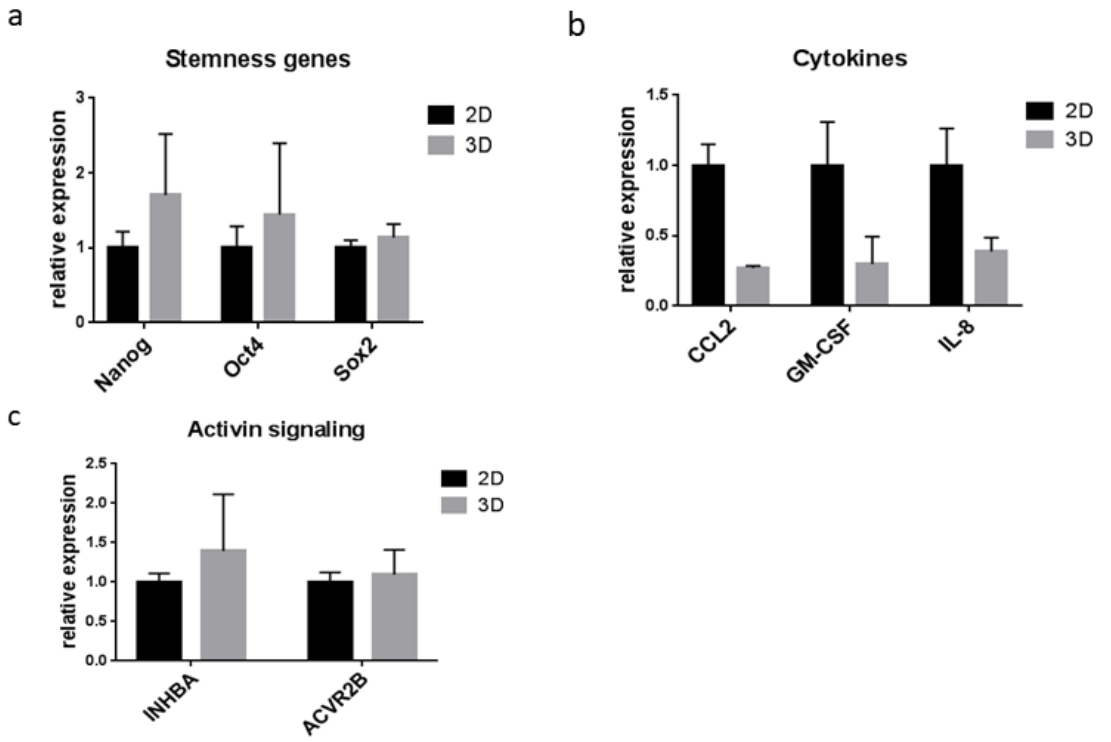

Suppl. Fig. 1 Upregulation of stemness genes, NF-κB dependent cytokines and INHBA in zebrafish is 3D context independent. (a-c) Expression of stemness genes NANOG, OCT4, SOX2, NF-κB dependent cytokines GM-CSF, CCL2, IL-8 and Activin A were compared between 2D and 3D cultures. (n=3)

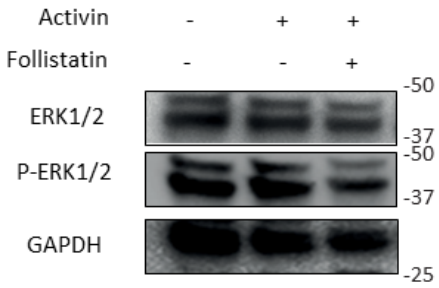

Suppl. Fig. 2 Treatment of Follistatin inhibits Activin A-induced ERK1/2 phosphorylation. PC-3M-Pro4 was respectively treated with veh, 100ng/ml Activin A and 100ng/ml Activin A plus 100ng/ml Follistatin for 24hours. Westenblot was performed to measure ERK1/2, p-ERK1/2 and GAPDH.

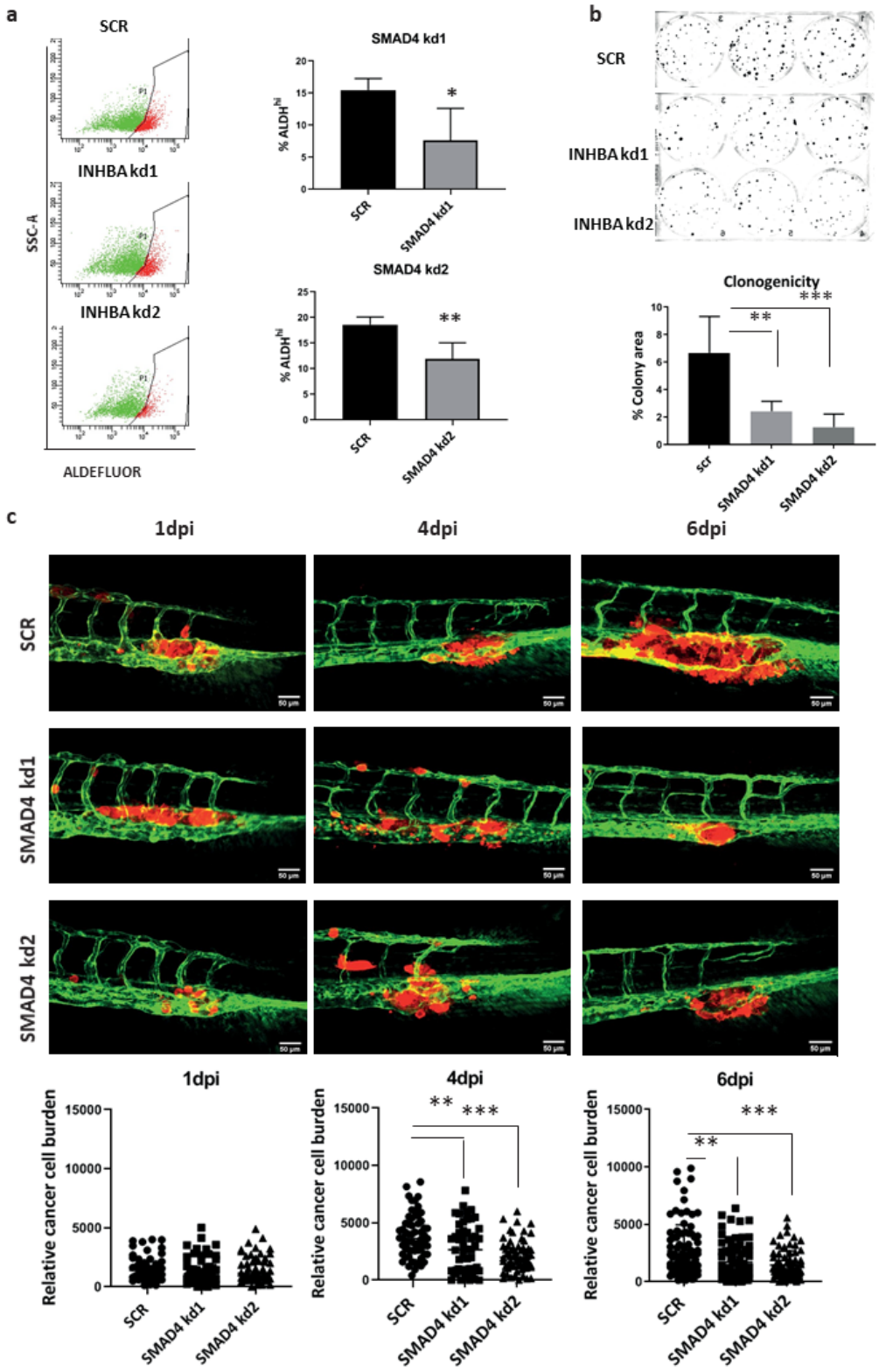

Suppl. Fig. 3 Knockdowns of SMAD4 inhibits ALDH^{hi} subpopulation and clonogenecity in vitro, and metastatic tumor growth in zebrafish xenografts.(a) ALDEFLUOR assay was performed to measure the size of ALDH^{hi} subpopulation in SCR, SMAD4 kd1 and SMAD4 kd2. (n=5 for SMAD4 kd1 and n=4 for SMAD4 kd2). (b) 300/well SCR, SMAD4 kd1 and SMAD4 kd2 cells were seed in 6 wells plate for 14 days. Size of total colony area was measured by Fiji. (n=6). (c) SCR, SMAD4 kd1 and SMAD4 kd2 cells were injected into ZF. Relative cancer cell burden at CHT area was measured at day1, day4 and day6 (n=60).

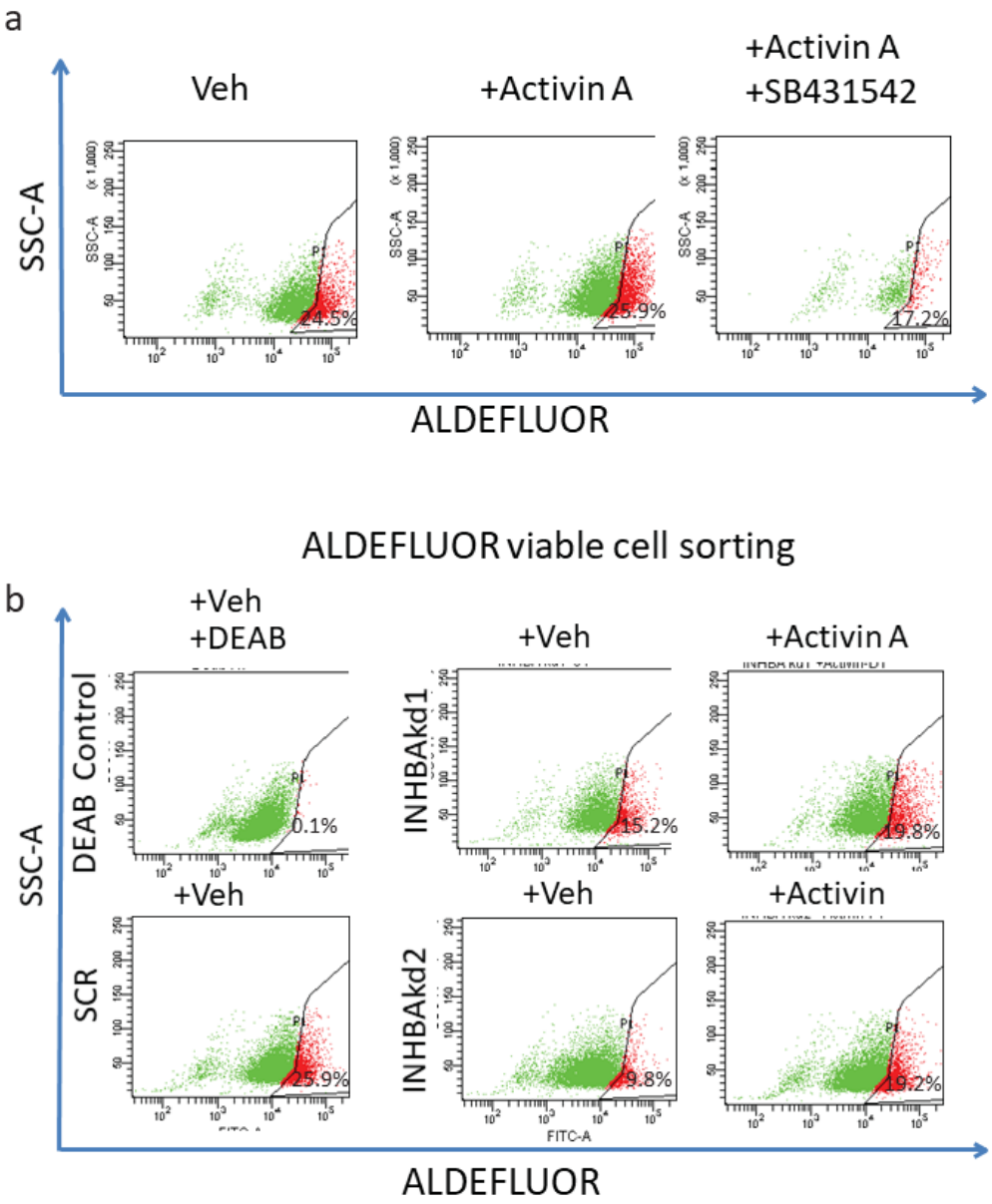

Suppl. Fig. 4 ALDEFLUOR assay to assess the effect of pharmacologic and genetic inhibition of Activin A in PC-3M-Pro4. (a) PC-3M-Pro4 cells treated with DEAB were used to gate the negative ALDH population. The cells with stronger ALDEFLUOR fluorescence than the DEAB treated cells were selected as $ALDH^{hi}$ cells (left top panel). The size of $ALDH^{hi}$ cells containing SCR non-targeting sequence (left bottom panel), INHBAkd1 and INHBAkd2 with or without Activin stimulation was measured (middle and right panel). (b) PC-3M-Pro4 cells were treated with Veh, Activin A and/or SB431542. The size of $ALDH^{hi}$ subpopulation was measured.

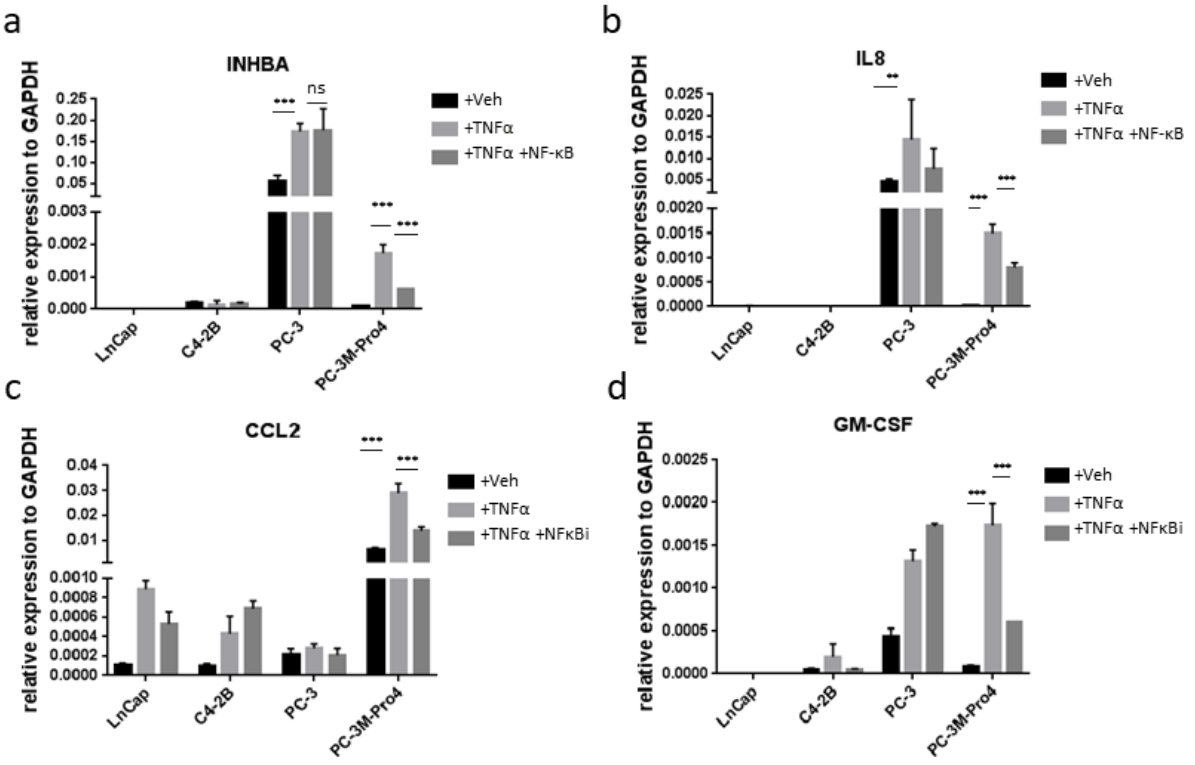

Suppl. Fig. 5 Expression of cytokines and INHBA is compared between PCa cell lines. (a-d) PCa cell lines LNCaP, C4-2B, PC-3 and PC-3M-Pro4 were treated with either Veh or TNFα for 24 hours. Expression of INHBA, IL-8, CCL2 and GM-CSF was detected by qPCR. Results were normalized to GAPDH expression (n=3).

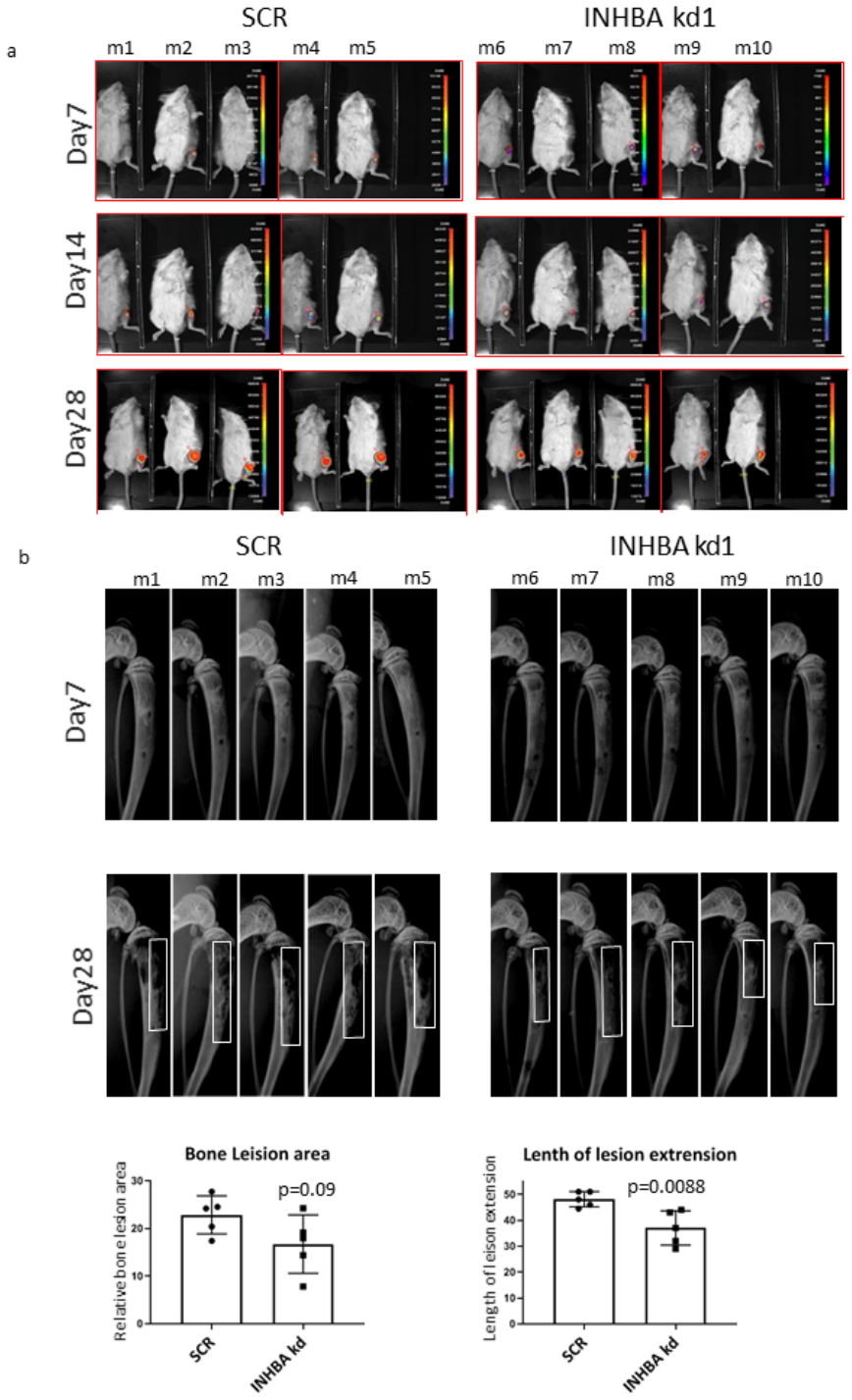

Suppl. Fig. 6 Overview of mice xenograft. (a) PC-3M-Pro4-Luc2-SCR and PC-3M-Pro4-Luc2-INHBAkd1 were injected into tibia of SCID CB17 mice. Tumor growth was monitored by bioluminescent imaging 7, 14 and 28 days after implantation. The INHBAkd significantly inhibited cell growth at day 14 and 28 (n=5, $p<0.05$). (b) INHBAkd inhibited the osteolytic lesion progression. Area and length of bone lesions were quantified using Fiji. Same animals displayed in (a). Square, Osteolytic lesion.